# RECENT RESEARCH ACTIVITIES

## The structural changes in cellulose microfibril and their susceptibilities to cellulase

**(Laboratory of Biomass Morphogenesis and Information, RISH, Kyoto University)**

Yoshiki Horikawa, Tomoya Imai, Kentaro Abe, and Junji Sugiyama

Lignocellulosic biomass is promising materials because of non-competition with food and it contains large amount of cellulose as a fermentable sugars. However, Cellulose is an insoluble crystalline polymer, which decreases the enzymatic hydrolysis from lignocellulose to monosaccharide. The efficient pretreatment, therefore, is required to enhance the susceptibility of cellulose by removing the matrix component as well as modification of cellulose structural property, which leading the reduction of enzyme dosage.

Therefore, we prepared well-dispersed microfibriller cellulose from *Eucalyptus globulus* by mechanical grinding and used as starting substrate [1]. The digestibility of this cellulose I achieves almost complete digestion when sufficient commercial cellulase loading as much as 20mg/g-substrate is applied. However, when the enzyme dosage is decreased to 2mg/g-substrate, the yield of digestion reaches the limit. Therefore, we have performed three pretreatment such as mercerization, dissolution into phosphoric acid and ethylenediamine (EDA) treatment. Transformation into cellulose II hydrate by mercerization and dissolution into phosphoric acid were not sufficient because substrate changed to highly crystalline structure during saccharification. On the other hand, in the case of crystalline conversion of cellulose I to $III_I$ by EDA, almost perfect hydrolysis was achieved even in enzyme loading as small as 0.5 mg/g-substrate, furthermore, hydrolyzed residue was changed to typical cellulose I (Figure), which clearly demonstrated cellulose I is more recalcitrant substrate compared to cellulose $III_I$. The structural analysis of substrate after digestion gives an insight into interaction of cellulose crystalline property and cellulase for better enzymatic digestion.

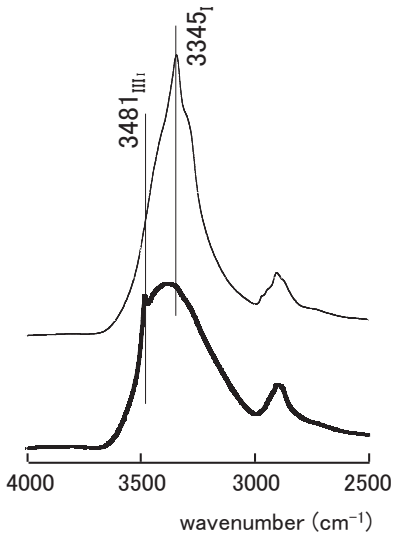


Figure FTIR spectra of cellulose $III_I$ before (bold line) and after enzymatic hydrolysis (hair line). The bands at 3345 and 3481 $cm^{-1}$ are specific to cellulose I and $III_I$, respectively.

**Acknowledgement**

The authors express their appreciation to Ms. K. Kanai and Ms. M. Imai for their technical support on the research. This study was supported by the New Energy and Industrial Technology Development Organization (NEDO).

**Reference**

[1] Horikawa, Y., Konakahara, N., Imai, T., Abe, K., Kobayashi, Y., Sugiyama, J. (2013) The structural changes in crystalline cellulose and effects on enzymatic digestibility. Polym. Degrad. Stabil., 98 (11), 2351-2356.

# RECENT RESEARCH ACTIVITIES

## Approaches towards wood biorefinery using whole cell wall components by microwave reactions

**(Laboratory of Biomass Conversion, RISH, Kyoto University)**

Takashi Watanabe

Production of biofuels, chemicals and materials from woody biomass is important for sustainable development of our society. In wood biorefinery including enzymatic saccharification and fermentation, lignin should be separated from the cell wall polysaccharides, accommodating increase in the hydrolyzability of (hemi)celluloses and use of the lignin as an aromatic feedstock [1]. To establish the environmentally friendly biorefinery process, we have been studying production of bioethanol and aromatic chemicals using microwave processing [2]. For industrial production of bioethanol, cost of the processing facilities should be minimized. In our NEDO project, we developed an ultra-low cost bench-scale microwave reactor which enabled highest level of energy transfer from commodity-use magnetrons to a reaction vessel without use of a matching tuner, isolator and power monitor [3]. A high-performance SHF and SSCF processes using ethanologenic bacteria, *Zymomonas mobilis* and *Zymobactor palmae* [4] and lignin-derived adsorbent for fermentation inhibitors have been developed for bioethanol production. We constructed a bench scale plant for the wood biorefinery (Figure 1), and demonstrated coproduction of bioethanol and lignin with minimum chemical modifications. The bioethanol produced was distilled, and its high quality as a transportation fuel and raw feedstock for propylene production was demonstrated.
As a value-added product from lignin, we studied production of ultraviolet (UV) absorbers by microwave reactions with Kao Corp. By extensive screening of degradation products from lignin, we isolated and identified lignin oligomers with high absorbance in UV-A and UV-B regions [5]. Recently we found that finely divided wood meal was dissolved in α-keto acid, pyruvic acid, and two aldehydic carboxylic acids, namely, glyoxylic acid and formic acid, at room temperature [6]. The wood solution was fractionated into cellulosic porous solid and other soluble components by addition of 2-methyltetrahydrofuran. The simple dissolution and separation technology coupled with the microwave processing in the presence of reaction catalysts will expand the wood biorefinery processes using whole cell wall components of wood.

**Acknowledgements**
We thank our collaborators, Prof. Hideshi Yanase, Tottori Univ., Japan Chemical Eng. and Machinery Co. Ltd. and Toyota Motors Corp. for NEDO bioethanol project. We acknowledge Dr. Tomohiko Mitani, Mr. Naoki Hasegawa, Prof. Naoki Shinohara, Dr. Koichi Yoshioka, Dr. Keigo Mikame, Dr. Hiroshi Nishimura and other members of the NEDO and CREST projects. We thank Mrs. Yuri Nishiwaki-Akine for the studies on dissolution and separation of woody biomass.
We also thank NEDO, JST and JSPS for financial support.

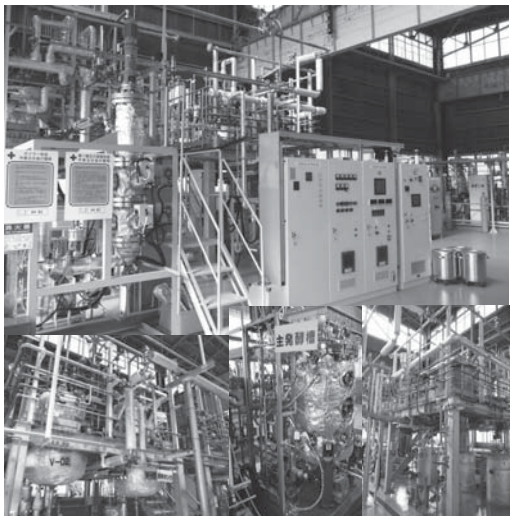

Figure 1 A bench-scale MW plant for 2nd generation bioethanol and biorefinery

**References**

[1] Watanabe, T., Introduction: Potential of Cellulosic Ethanol, In Lignocellulose Conversion, Chapter 1; V. Faraco Ed.; Springer: New York, pp.1-20 (2013).
[2] Watanabe, T. and T. Mitani, Microwave technology for lignocellulosic biorefinery, In The Role of Green Chemistry in Biomass Processing and Conversion, eds. by H. Xie, N. Gathergood, John Wiley & Sons, 281-291 (2012).
[3] Hasegawa, N. et al., IEICE Transactions, in press (2014).
[4] Yanase, H., et al., *Appl. Microbiol. Biotechnol.,* **94**, 1667–1678 (2012**)**.
[5] JP A2012-056100
[6] Nishiwaki-Akine, Y. and T. Watanabe, *Green Chem.*, **16**, 3569-3579 (2014).

RECENT RESEARCH ACTIVITIES

# Characterization of cell wall phenylpropanoids of grass bioenergy plants and characterization of ubiquitin ligase involved in secondary cell wall formation in *Arabidopsis*

**(Laboratory of Metabolic Science of Forest Plants and Microorganisms, RISH, Kyoto University)**

Masaomi Yamamura, Shiro Suzuki, and Toshiaki Umezawa

## 1. Characterization of cell wall phenylpropanoids of grass bioenergy plants

Lignocelluloses are produced mainly by trees and large gramineous plants such as *Erianthus* spp., switchgrass, nepier grass, miscanthus etc. Because large gramineous plants produce large amounts of biomass, do not compete with food, and can grow under a wide range of conditions, they are drawing attention as potential materials for biofuel and industrial feedstock production. Generally, both lignin and ferulate (or diferulate) cross-linking in the cell wall are known as obstructive factors in the enzymatic saccharification process for the production of biofuel. This study established a system to quantitate diferulates in cell walls of various grass energy plants using stable isotope dilution method.

In this study, various deuterium-labeled and unlabeled diferulates were synthesized, and it was shown that some diferulates are rather unstable; the unstability was partially eliminated by the introduction of protecting groups: acethylation of the phenolic hydroxyls and ethyl ester formation from the carboxyls. In addition, it was shown for the first time that the amounts of diferulates in cell wall materials of *Erianthus arundinaceus* were very small. The present result suggested that the role of the diferulate residues as the obstacles of enzymatic saccharification of *E. arundinaceus* internodes may be insignificant [1].

## 2. Characterization of ubiquitin ligase involved in secondary cell wall formation in *Arabidopsis*

Recently, many transcription factors which coordinately regulate biosynthesis of the secondary wall components have been uncovered in a model dicotyledonous plant *Arabidopsis thaliana*. However, little was known about other regulatory systems of secondary wall formation. The present study indicated that an E3 ubiquitin ligase, which plays an important role in the selective protein degradation via the ubiquitin-proteasome pathway, was involved in secondary wall formation.

Using a gene co-expression network analysis, we found that *Arabidopsis Tóxicos en Levadura54* (*ATL54*, At1g72220) encoding a putative ubiquitin ligase was co-expressed with some genes involved in secondary wall formation. The recombinant ATL54 protein catalyzed E1- and E2-dependent auto-ubiquitination. Expression of some biosynthetic genes of secondary wall components was up-regulated in apical stem portions of the *ATL54*-knock-out mutants, while expression of a gene involved in programmed cell death of tracheary elements was significantly repressed in both *ATL54*-knock-out and *ATL54*-overexpressed mutants. Moreover, we found that the *β-glucuronidase* (*GUS*) reporter gene driven by the *ATL54* promoter was significantly expressed in interfascicular fibers, xylary fibers, and vessels in inflorescence stems. The dual luciferase transient transfection assay demonstrated that *ATL54* was transactivated by MYB46, a master regulator of secondary wall biosynthetic genes. An electrophoretic mobility shift assay showed that MYB46 directly bound to *ATL54* promoter fragments. These results suggested that ATL54 was an E3 ubiquitin ligase involved in secondary wall biosynthesis and programmed cell death during xylogenesis [2], and indicated that *ATL54* expression was directly regulated by MYB46 [3] .

**References**

[1] Yasui A, Yamamura M, Suzuki S, Umezawa T (2013) “Establishment of the system to measure diferulates in the cell wall of gramineous plants”, The 63rd Annual Meeting of the Japan Wood Research Society (in Matsuyama)

[2] Noda S, Takahashi Y, Tsurumaki Y, Yamamura M, Nishikubo N, Yamaguchi M, Sakurai N, Hattori T, Suzuki H, Demura T, Shibata D, Suzuki S, Umezawa T (2013) ATL54, a RING-H2 domain protein selected by a gene co-expression network analysis, is associated with secondary cell wall formation in *Arabidopsis*. *Plant Biotechnol* 30: 169–177

[3] Noda S, Yamaguchi M, Tsurumaki Y, Takahashi Y, Nishikubo N, Hattori T, Demura T, Suzuki S, Umezawa T (2013) ATL54, a ubiquitin ligase gene related to secondary cell wall formation, is transcriptionally regulated by MYB46. *Plant Biotechnol* 30: 503–509

# RECENT RESEARCH ACTIVITIES

## Coumarin-specific prenyltransferase, an enzyme crucial for furanocoumarin biosynthesis in parsley

**(Laboratory of Plant Gene Expression, RISH, Kyoto University)**

Akifumi Sugiyama, Kojiro Takanashi and Kazufumi Yazaki

Furanocoumarins constitute a class of phenolic plant secondary metabolites, which are essentially found in four higher-plant families (Apiaceae, Rutaceae, Fabaceae and Moraceae). Furanocoumarins are important protectants for plants against pathogens or insects. In addition franocoumarins contribute to inter-specific competition by inhibiting the germination and growth of neighboring plants. In parsley (*Petroselinum crispum*), these compounds preferentially accumulate in oil ducts.

The metabolic profile of furanocoumarin differs largely depending on plant species, the age, and the tissues. There are two types of furanocoumarins derived from two parallel biosynthetic pathways, i.e., linear and angular furanocoumarins. It is hypothesized that these two pathways emerged from the result of co-evolution between plants and insects. Researches on interactions between butterfly larvae (*Depressaria pastinacella*) and an Apiaceae plant *Pastinaca sativa* showed that angular franocoumarins display a synergistic effect with linear ones, contributing the mixtures of linear and angular compounds more difficult for insects to detoxify. Thus, angular furanocoumarins have been hypothesized to appear later than linear ones over the course of plant evolution. This hypothesis is in line with the fact that angular furanocoumarins are always found concomitantly with linear structures in the plant kingdom.

The prenylation position of the common precursor of all furanocoumarins, umbelliferone, determines the type of furanocoumarin. Prenylation at C6 and C8 gives rise to the psoralen or angelicin derivatives, respectively. In this study, we identified a membrane-bound prenyltransferase PcPT from parsley, and characterized the enzymatic properties. PcPT expression in various parsley tissues is induced by UV irradiation, with a concomitant increase in furanocoumarin production *in planta*. PcPT has strict substrate specificity towards umbelliferone and dimethylallyl diphosphate, and a strong preference for the C6 position of the prenylated product (demethylsuberosin), which leads to the biosynthesis of linear furanocoumarins. In addition to the C6-prenylation, this enzyme also catalyzes the C8-prenylation in a much lesser extent. The PcPT protein was shown to be targeted to the plastids *in planta*. Metabolic engineering was performed in coumarin-producing plant *Ruta graveolens*, in which *PcPT* gene was over-expressed. It was found that PcPT expression in *Ruta graveolens* increased consumption of endogenous umbelliferone. Expression of PcPT together with a 4–coumaroyl CoA 2'–hydroxylase gene in *Nicotiana benthamiana*, which does not produce furanocoumarins, resulted in the formation of demethylsuberosin, indicative that furanocoumarin production may be reconstructed in non-producing plants. This finding suggested the plasticity of the furanocoumarin pathway, in particular for the emergence of angular structures during the course of plant evolution.

**Acknowledgements**

We are grateful to D. Baulcombe (University of Cambridge, UK) for pBIN61–P19, T. Nakagawa (Shimane University, Japan) for pGWB vectors, T. Mitsui (Niigata University, Japan) for WxTP–DsRed, H. Kouchi (National Institute of Agrobiological Sciences, Japan) for pHKN29 (GFP), and T. Duval (University of Lorraine, France) for technical assistance.

**Reference**

F. Karamat, A. Olry, R. Munakata, T. Koeduka, A. Sugiyama, C. Paris, A. Hehn, F. Bourgaud, K. Yazaki, “A coumarin-specific prenyltransferase catalyzes the crucial biosynthetic reaction for furanocoumarin formation in parsley,” *The Plant Journal*, vol. 77, no. 4, pp. 627-638, 2014.

# RECENT RESEARCH ACTIVITIES

## Equatorial MU Radar (EMU)
## Equatorial fountain in the middle and upper atmosphere over Indonesia

**(Laboratory of Atmospheric Sensing and Diagnosis, RISH, Kyoto University)**

Toshitaka Tsuda

We are studying the coupling process in the solar-terrestrial system, focusing on the solar energy inputs into the Earth, and the response of the atmosphere to energy input. The solar energy can mainly be divided into two parts: the solar radiation involving infra-red, visible, ultra-violet and X-ray, and solar wind which is a high-speed flow of plasma particles. Electro-magnetic energy due to solar wind converges into the polar region, while, the solar radiation becomes maximum at the equator and atmospheric disturbances are actively generated near the Earth's surface. In particular, over Indonesia cumulonimbus convection is most active in the world. It further excites various atmospheric waves that propagate upward to transport energy and momentum into the upper atmosphere. Also, different kinds of materials (atmospheric minor constituents) originating at low- and mid-latitude regions converging into the equatorial region, are blown upward through the tropopause at about 15 km into the middle atmosphere (10-100 km), and spread to the whole globe. In the upper atmosphere, plasma disturbances and equatorial ionization anomaly are generated around the equator.

A number of international collaborative programs on the coupling processes in the solar-terrestrial system have been coordinated under SCOSTEP of ICSU. We have contributed much to these programs through observations especially using a state-of-the-art large atmospheric radar that enables us to study the behavior of the troposphere (altitude up to 10-15 km), middle atmosphere (10-100 km) and upper atmosphere (above 100 km). We have developed the middle and upper atmosphere radar (MU radar) in Shigaraki, Japan in 1984, the Equatorial Atmosphere Radar (EAR) right over the equator in West Sumatra, Indonesia in 2001. We are now promoting to construct the Equatorial MU Radar (EMU), which will be 10 times more sensitive than EAR. We will capture the energy and material flow that occur in all height ranges of the equatorial atmosphere as "Equatorial Fountain" using EMU.

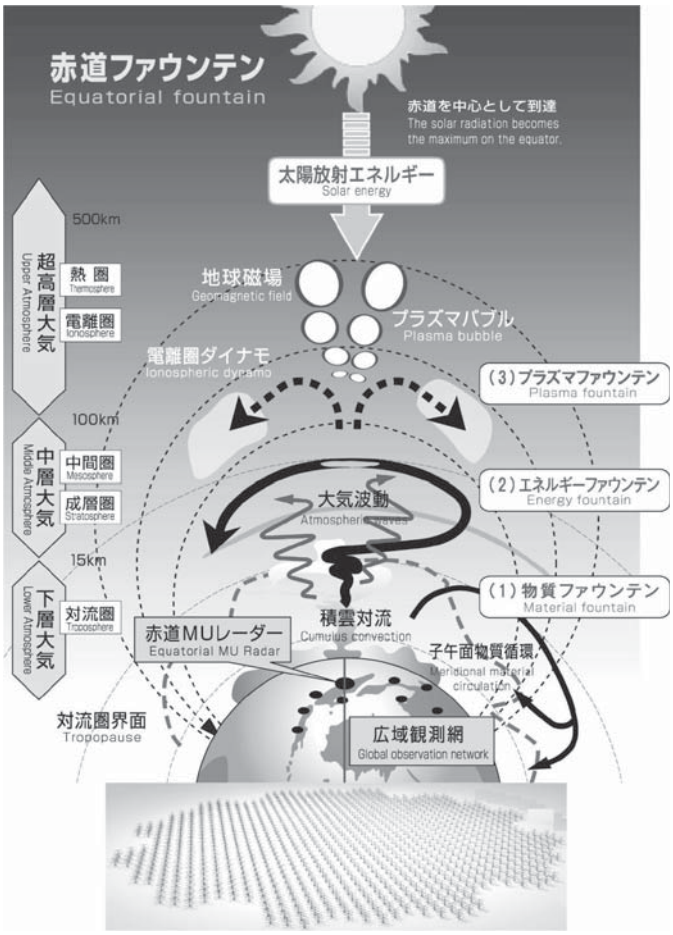


Figure 1. The energy and material flows that occur in all height regions of the equatorial atmosphere are named as “Equatorial Fountain”, which will be studied with the EMU.

# RECENT RESEARCH ACTIVITIES

## Diurnal ozone variations in the stratosphere as revealed by SMILES measurements

**(Laboratory of Atmospheric Environmental Information Analysis, RISH, Kyoto University)**

Takatoshi Sakazaki

Since the discovery of the ozone hole, stratospheric ozone has been extensively investigated over the last 30 years; however, the global structure of diurnal variations in stratospheric ozone remains unclear, particularly for the lower to middle stratospheric ozone that mainly contributes to total column ozone.

Superconducting Submillimeter-Wave Limb-Emission Sounder (SMILES) were launched in September 11, 2009 and attached to the Japanese Experiment Module (JEM) onboard the International Space Station (ISS). The SMILES achieved an exceptionally precise observation of atmospheric minor constituents (e.g., ozone) between October 2009 and April 2010. The resulting precision is one-order of magnitude better than that from many other satellite measurements. Also, SMILES can measure the atmosphere at different local times because of the non-Sun-synchronous ISS orbit.

By using the SMILES data, we, for the first time, observationally revealed the global pattern of diurnal ozone variations throughout the stratosphere (Figure 1) [1]. We found that the peak-to-peak difference in stratospheric ozone profiles (total column ozone) is up to 8% (1%) over the course of a day. In addition, these results were quantitatively reproduced by nudged chemistry-climate models. An analysis of the model output showed that the diurnal variations are due to dynamical processes (vertical transport by atmospheric tidal winds) as well as photochemical processes.

Our findings could lead to correct bias in satellite measurements that are caused by the difference in local time of measurements. In fact, we showed that the diurnal variations could explain the 'sunset-sunrise differences in ozone amount' reported in several solar occultation measurements (N.B. Solar occultation instruments make measurements only at sunrise and sunset) [2].

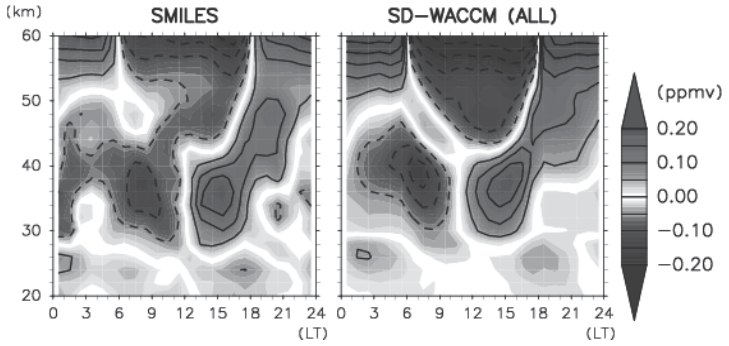


Figure 1. Local-time versus altitude distribution of diurnal ozone variations (ppmv) averaged between 10°S and 10°N, as derived from data by (left) SMILES observations and (right) chemical transport model simulations (SD-WACCM).

**References**

[1] Sakazaki, T., M. Fujiwara, C. Mitsuda, K. Imai, N. Manago, Y. Naito, T. Nakamura, H. Akiyoshi, D. Kinnison, T. Sano, M. Suzuki, and M. Shiotani, "Diurnal ozone variations in the stratosphere revealed in observations from the Superconducting Submillimeter-Wave Limb-Emission Sounder (SMILES) on board the International Space Station (ISS)." *Journal of Geophysical Research*, 118, 2991-3006, doi:10.1002/jgrd.50220, 2013.

[2] Sakazaki, T., M. Shiotani, M. Suzuki, D. Kinnision, J. M. Zawodny, M. McHugh, and K. Walker, "Sunset-sunrise difference in solar occultation measurements (SAGE II, HALOE, and ACE-FTS) and its relationship to tidal vertical winds", *Atmos. Chem. Phys. Discuss.,* 14, pp. 16043-16083, 2014.

# RECENT RESEARCH ACTIVITIES

## Development of a digital receiver for imaging atmospheric radars

**(Laboratory of Radar Atmospheric Science, RISH, Kyoto University)**

Masayuki Yamamoto, Tong Gan, Hiroyuki Hashiguchi, and Mamoru Yamamoto

Radar imaging is a technique that enhances radar range and angular resolution using multiple frequencies and receivers. MU radar, which has the capability of radar imaging, has demonstrated that radar imaging is indispensable for resolving fine-scale dynamical processes caused by atmospheric instabilities. Further, additional use of auxiliary sub-arrays contributes to reduce undesired received signals (i.e., clutter signals) from the ground and flying objects (aircrafts, birds, and insects). However, atmospheric radars which have the capability of radar imaging are not common. In order to implement radar imaging capability to the existing atmospheric radars, a digital receiver with a low purchase cost, high-rate sampling capability of received signals, and configurable real-time signal processing, is necessary.

In order to implement radar imaging capability to the Equatorial Atmosphere Radar (EAR) installed in Indonesia, we are now developing a digital receiver. Figure 1 shows a schematic diagram of the digital receiver for the EAR. The digital receiver comprises of two general-purpose software radio receivers (USRP produced by Ettus Research) and a personal computer (PC). In order to start sampling of received signals, transmission trigger pulse (TX trigger pulse) supplied by the EAR is collected by the USRP. Another USRP is used to sample IF received signals. In order to synchronize the transmission and reception frequencies of the EAR, 10-MHz reference and 1 pulse per second (PPS) signals supplied by the EAR are used.

By installing the single digital receiver, the EAR attains oversampling (OS) capability up to 10 mega-samples per second. OS is useful for improving the vertical resolution using radar imaging. After enhancing the vertical resolution, we will install the multiple digital receivers for enhancing the angular resolution and for reducing clutter signals. Implementation of the digital receiver to other atmospheric radars is also carried out.

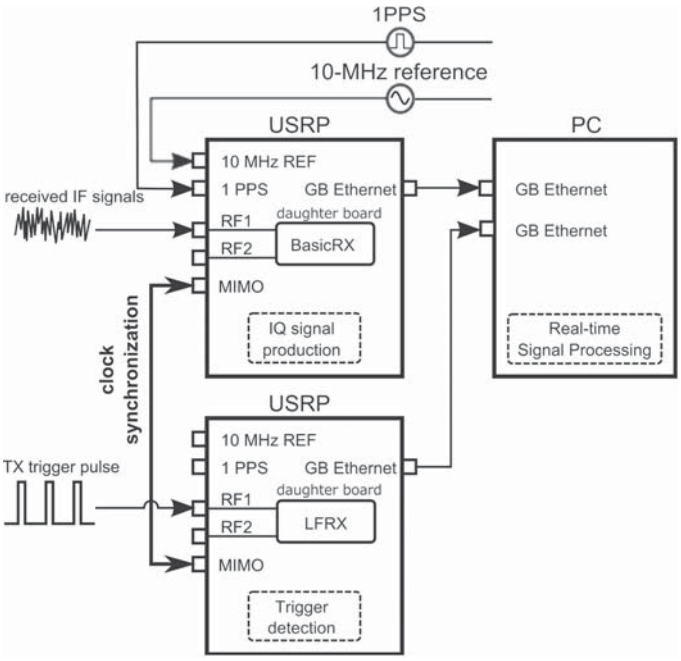


Figure 1. Schematic diagram of the digital receiver.

# RECENT RESEARCH ACTIVITIES

## Transparent paper: A paradigm from nanofibers to nanostructured fibers

**(Laboratory of Active Bio-based Materials, RISH, Kyoto University)**

Hiroyuki Yano, Shouzou Sasaki, Md. Iftekhar Shams, Kentaro Abe and Takeshi Date

In the digital era, ample information is being exchanged through electronic media and the demand for high-quality, smart, and portable digital devices is increasing sharply. Because of its very low coefficient of thermal expansion and transparency, glass has up to now been used extensively in the substrates of electronic devices such as displays and solar cells. However, in modern flat panel display (FPD) technology and solar cell production, continuous "roll-to-roll" (RTR) processing using flexible plastic substrates is expected to take over from conventional "batch" processing of glass substrates. Plastic is no doubt a good choice for flexible displays and solar cells. However, practical RTR processing has so far been prevented by the high coefficient of thermal expansion (CTE) of the plastics to be used. One possible way to reduce thermal expansion while only causing a low loss in transparency would be to use fillers with a diameter significantly smaller than the wavelength of visible light. Nanofibers are believed to have the potential to substantially improve the mechanical properties of polymers.

Cellulose nanofibers 4 to 20 nm in width, the major component of the plant cell wall and the most abundant bio resources on earth, have received great interest because of their outstanding mechanical properties due to their high molar mass and highly ordered extended chain polysaccharide nanofiber structures. This makes it a preferable candidate for RTR manufacturing processes because no discrepancy between the CTEs of the different materials used will arise. However, nanofibers production is high in energy consumption. Therefore, we developed a low thermally expanded transparent film by exploiting wood fibers that can be considered to be nanostructured fibers in which individual nanofibers do not significantly agglomerate. We thereby demonstrate that paper, used since ancient times, will be a next-gen optical material.

After removing lignin and hemicelluloses from wood pups, generation of hydrogen bonding among cellulose nanofibers in the wood pulp must be avoided. In this study, the wood pulps were acetylated with much care taken to maintain a never dried state. Furthermore, we attempted internal fibrillation using bead-mill of the pulp before acetylation. The moisture content of untreated pulp and acetylated pulp did not even change after fibrillation. As a result, the fibrillated acetylated pulp composites (thickness: 50 μm, fiber content: 17.1%) displayed 84.2% light transmission at a wavelength of 600 nm, as shown in and Figure 1. Despite the heterogeneous structure consisting of pulp of some one-tenth micrometer in width, the difference in the regular optical transmittance compared with that of the acetylated cellulose nanofiber composites was small.

Figure 1. Wood pulp-based optically transparent nanocomposite.

The fibrillated acetylated pulp also enabled a reduction in the CTE of the composites. The addition of 24.5 wt% fibrillated acetylated pulp reduced the CTE of acrylic resin from 213 ppm/K to 13.1 ppm/K. This is 4 times more than the untreated pulp composites and 1.4 times more than the untreated fibrillated pulp composites. This is apparently due to the decrease in the number of fiber-fiber interactions caused by decreased intrafibrillar hydrogen bonding between pulps. However, interestingly, this value is comparable to the CTE of acetylated cellulose nanofiber-reinforced acrylic resin (12.1 ppm/K) with higher cellulose content such as 40%. This inspiring optically transparent and extremely low thermal expansion film could be fabricated through traditional paper manufacturing process, and thus is exceedingly closer to industrial application with prospects ready to be realized.

**References**

[1] Yano H, Sasaki S, Shams MI, Abe K, Date T, "Wood pulp based optically transparent film: A paradigm from nanofibers to nanostructured fibers", *Advanced Optical Materials*, 2 (3), 231-234, 2014

RECENT RESEARCH ACTIVITIES

# Investigation of a new natural particleboard adhesive composed of tannin and sucrose

**(Laboratory of Sustainable Materials, RISH, Kyoto University)**

Zhongyuan Zhao and Kenji Umemura

In the face of dwindling fossil fuel resources and the environmental imperative to reduce emissions associated with petrochemistry, there is strong demand for a wood composite bonding procedure using natural alternatives. Our laboratory carried out a series of the research on the natural adhesives. In this study, particleboards were manufactured with a new material adhesive composed of tannin and sucrose (as Figure 1 shows), and the ratio of tannin and sucrose was 25/75 with the concentration of solution at 40wt%. The boards were hot-pressed for 10 min. The size of the board was 300×300×90mm and the target density was 0.8 g/cm3. The effects of the resin contents and hot pressing temperature on the physical properties of the resulting particleboard were investigated.

**Materials**

Recycled wood particles were dried in oven at 80°C for 12h. Wattle tannin (Fuji Chemical Industry Co.) and sucrose(Nacalai Tesque, Inc. ) were dried in vacuum oven at 60°C for 15h.

**Evaluation of particleboard**

The boards obtained were conditioned for 1 week at 20 °C and RH 60%. The static 3-point bending test, the internal bond strength (IB) test and thickness swelling (TS) test were carried out.

**Effects of resin content**

Particleboards were manufactured with the resin content at 10, 15, 20, 30 and 40wt%. Both MOR and MOE were slightly enhanced with the increase of resin content. The maximum average values of MOR and MOE were 21.2 MPa and 5 GPa, respectively, obtained at 40wt% resin content case. The IB strength performance did not change obviously with changes in resin content. The maximum average value was 1.3 MPa at resin content of 30wt%. The TS value decreased as the resin content increased. The lowest value of TS was 20% with 40wt% resin content. Based on the results above, the optimum resin content was between 30 to 40wt%.

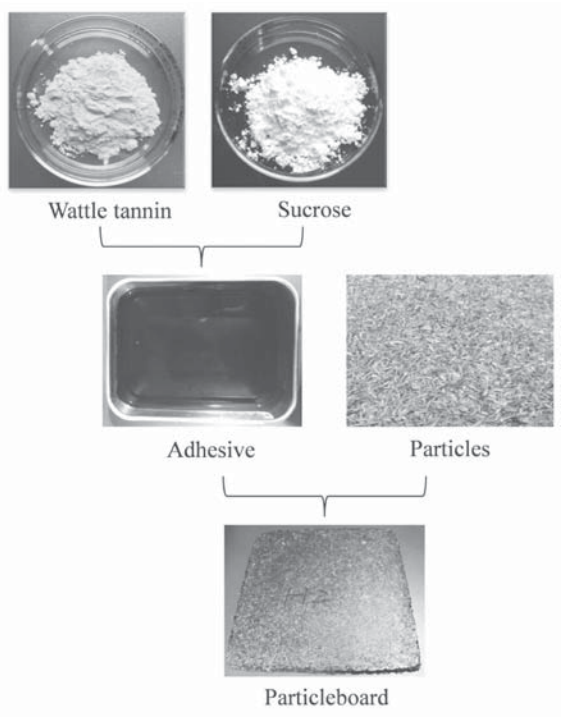


Figure 1. The manufacture of the particleboard bonded with tannin and sucrose

**Effects of hot pressing temperature**

Particleboards were manufactured with the hot pressing temperature at 160, 180, 200 and 220℃. The maximum value of MOR and MOE were 21.9MPa and 4.95GPa, respectively, when the board was bonded with 40wt% resin content at 220℃. The maximum value of IB was 1.6MPa from the board bonded with 40wt% resin content and 220℃. When the board bonded with 30 and 40wt% resin content at 220℃, the TS values were 9.6 and 7.3%, respectively, this value satisfied requirement of 18 type of JIS A 5908. The results obtained above indicated that, when the hot press temperature increased to 220℃, the particleboard board bonded with tannin and sucrose performed excellent mechanical properties and water resistance.

# RECENT RESEARCH ACTIVITIES

## Pull-out strength properties of Lagscrewbolt connection for CLT construction

**(Laboratory of Structural Function, RISH, Kyoto University)**

Takuro Mori, Hiroshi Isoda, Akihisa Kitamori

With the availability of new engineered wood products such as cross laminated timber (CLT), it becomes possible to build a wide variety of wooden construction of frame structures of large height and long span. One of the most important design aspects for these structures is the connection. The lagscrewbolt (LSB) was first developed by Komatsu [1] as a rigid connector for wooden structures. A lot of the research was done with a focus on use of LSB in glulam construction.

This study was aimed at examining the structural performance of a single or double LSBs inserted into CLT in terms of the insertion direction, the edge distance, and the distance of both LSBs. In Figure 1 was shown the LSB and CLT. The several parameter's specimens were tested for evaluating this aims.

In this report, many types of specimens were used to examine the effect of edge distance, grain direction and multiple LSBs. It could be concluded as follows:

Figure 1. Shape of a Lagscrewbolt and Cross Laminated Timber

1. The pull-out strength of LSB when inserted through the perpendicular-to-grain direction with enough resisting area into CLT layers was higher than that when inserted in the parallel-to-grain direction, but the stiffness showed an opposite trend; the narrower specimens failed in a less ductile manner than wider ones; and the in-between inserting specimen had both strength and stiffness values between the perpendicular and parallel specimens. These results showed the same tendency as those in Glulam.
2. When inserted through the perpendicular-to-grain direction, it was found that the edge distance should be larger than 4d, and when using double LSBs, the strength and energy absorption decreased compared with single ones.
3. When inserted through the parallel-to-grain direction, it seemed that a 2d edge distance was not enough, because of failure mode. Therefore, to insert LSB more than 2d edge distance is recommended.
4. It was found that the formula in CLT Handbook and NDS for calculating the pull-out strength of lag screws was promising to adopt on perpendicular-to-grain direction.

It is recommended to conduct future work: to investigate the effect of edge distance and the distance between LSBs when increasing the inserting length; and to develop a prediction model or experimental formula for LSB connection in CLT.

**Acknowledgements**

This work was supported by the Kyoto University Global Frontier Project for Young Professionals: the John Mung Program, NSERC Strategy Research Network NEWBuildS (Canada), and Y. H. Chui and Meng Gong the Wood Science and Technology Centre, the University of New Brunswick, Canada.

**References**

[1] K. Komatsu, Y. Hara, Y. Nanami, and T. Ikki: Development of Lagscrewbolt as a connector for Glulam moment-resisting joints, *Proceedings of Pacific Timber Engineering Conference*, pp.2.349-2.354, Rotorua, New Zealand, 1999.

# RECENT RESEARCH ACTIVITIES

## Role of Termites in the Soil Nutritional Ecosystem of Temperate Regions

**(Laboratory of Innovative Humano-habitability, RISH, Kyoto University)**

Tsuyoshi Yoshimura

Termites are dominant soil animals in the tropics and sub-tropics [1], and play a major role in the soil nutritional ecosystem by recycling ligno-cellulosic materials and minerals [1]. In addition, soils of termite mounds, which are abundant source in tropical areas, are known to be beneficial materials for human as soil fertilizer [2] and wall materials of houses [3].

In contrast, ecological role of termites in temperate countries are not well understood. It is mainly due to their notorieties as the most important pest for houses. The simple calculation of termite population in urban landscapes of Japan, which is based on the infestation rate of houses [4], reveals that on average more than 100 individuals are living in $1m^2$. We, thus, have just started the international collaborative research on role of termite in the soil nutritional ecosystem of temperate regions.

In Japan, the monitoring devices, PVC pipe with a removable cap on the top and wooden feeder stakes, were set-up in the Living-sphere Simulation Field (LSF) site of Kyoto University near coastline in Hioki City, Kagoshima Prefecture in 2013. LSF site is located in planted pine forest area. Another 2 monitoring sites are located in suburban planted pine forest fragments in Uji campus of Kyoto University. Four additional monitoring sites, which are dominated with planted Hinoki (*Chamaecyparis obtusa*), Konara (*Quercus serrate*), Akamatsu (*Pines densiflora*), Akamatsu-Soyogo (*Ilex pedunculosa*), are in a secondary forest on Ryukoku-no Mori near Ryukoku University in Otsu City, Shiga Prefecture in 2014. In the USA, similar devices were set-up in planted pine forests in suburban.

After 5 - 6 months, the monitoring devices are surveyed and the following samples are collected: a) termite mud-tubes attached on the surface of the wooden stakes, b) termites, c) 10-cm depth soil samples 1-m apart from the monitoring devices. Termites are kept with water saturated wood blocks for 2 weeks to obtain frass samples. All the samples are served for the CHN analysis (organic materials) and the ICP analysis (minerals) after the pre-treatment.

The preliminarily results from the USA (Forschler, unpublished data) showed that there were 3 types in elements as follows: i) K, C, N, Na, Mn, Mg, B: the higher concentrations in the termite-related samples than in a soil sample, ii) P, Zn, AL, Cu: the lower concentrations in the termite-related samples than in the soil samples, iii) Cd, Co, Ca, Fe: similar levels in both the sample. In Japan, termites were collected from 34 out of 72 monitoring devices (47%) in the LSF site with 22 frass samples. All the collected samples are now under the pre-treatment for the analyses.

**Acknowledgements**

The author thanks to Prof. Brian T. Forschler and Ms. Yi-An Chen of the University of Georgia, and Prof. Ryunosuke Kikuchi and Mr. Shuhei Kimua of Ryukoku University for their collaboration in this research project. The appreciation also goes to Mr. Kosuke Nakayama of Ryukoku University, and Mr. Akio Adachi, Ms. Izumi Fujimoto, Ms. Kazuko Ono, Mr. Baek-Yong Choi and Mr. Khoirul Himmi Setiawan of RISH for their helps in preparing and setting-up the devices.

**References**

[1] Abe, T, “Ecology of Termites”, The University of Tokyo Press, 1989

[2] Miyagawa, S. et al., “Indigenous utilization of termite mounds and their sustainability in a rice growing village of the central plain of Laos,” *J. Ethnobiol. Ethnomedicine*, vo.7, no.24, pp.1-6, 2011.

[3] Yamashina, C. “Utilization of termite mounds by people living in the north-eastern Namibia,” *Zairaichi*, vol.1, pp.15-24, 2006 (in Japanese).

[4] The Japan Termite Control Association, “The report on termite infestation in Japan”, 2004

# RECENT RESEARCH ACTIVITIES

## Simulations and Modeling of Geospace Environment

**(Laboratory of Computer Space Science, RISH, Kyoto University)**

Yoshiharu Omura and Yusuke Ebihara

The Earth is surrounded by the radiation belts that consist of relativistic electrons. The growth and decay of the radiation belts come from the competition between generation and loss processes of energetic electrons. We conducted test particle simulations with a large number of relativistic electrons interacting with electromagnetic ion cyclotron (EMIC) triggered emissions. A substantial amount of relativistic electrons is trapped by the EMIC wave, and guided to lower pitch angles within a short time scale. We demonstrated that the relativistic electrons are efficiently precipitated into the atmosphere, resulting in a rapid loss of the radiation belt [1]. The coherent EMIC triggered emissions are well reproduced by energetic protons with large temperature anisotropy. The optimum wave amplitude and the transition from a linear stage to a nonlinear stage are in a good agreement with theory. A subpacket structure appears because of a new triggering wave [2]. The EMIC waves are found in the deep inner magnetosphere at L=2.5 − 5, based on observations by the Akebono satellite. The mode conversion and rising tone structures are clearly identified, which are consistent with theory [3].

Plasma circulates in the magnetosphere, which is called a magnetospheric convection. As a consequence, hot plasma is transported from the plasma sheet on the nightside into the inner region, resulting in the formation of the ring current and the seed of the radiation belt. A substorm, which is one of the most severe disturbances in the magnetosphere, is known to rapidly supply the hot plasma into the inner magnetosphere. During the interval of a substorm, magnetic field lines are shortened. This is called dipolarization. We found that the dipolarization process does not proceed smoothly during a substorm, and that the electric field oscillates with a period of 2–3 min, resulting in multiple enhancements of low-energy electrons in the course of a substorm [4]. The characteristics of the multiple enhancements of electrons are consistent with observations, and found to be a natural consequence of the force imbalance, not simply due to multiple injections. We also demonstrated for the first time that the direction of the convection electric field is reversed just after a substorm. General tendency of ground magnetic disturbances from pole to equator is similar to that observed. This implies that a substorm is not a simple element of magnetic storms as was suggested about a half century ago because the reversal of the convection impedes transportation of hot plasma from the nightside plasma sheet. The reversal of the convection results from the mutual coupling between the magnetosphere and the ionosphere.

### References

[1] Omura, Y. and Q. Zhao, Relativistic electron microbursts due to nonlinear pitch-angle scattering by EMIC triggered emissions, J. Geophys. Res., 118, 5008–5020, doi: 10.1002/jgra.50477, 2013.

[2] Shoji, M. and Y. Omura, Triggering process of electromagnetic ion cyclotron rising tone emissions in the inner magnetosphere, J. Geophys. Res., 118, 5553–5561, doi:10.1002/jgra.50523, 2013.

[3] Sakaguchi, K., Y. Kasahara, M. Shoji, Y. Omura, Y. Miyoshi, T. Nagatsuma, A. Kumamoto and A. Matsuoka, Akebono observations of EMIC waves in the slot region of the radiation belts, Geophys. Res. Lett., 40, doi: 10.1002/2013GL058258, 2013.

[4] Ebihara, Y. and T. Tanaka, Fundamental properties of substorm-time energetic electrons in the inner magnetosphere, J. Geophys. Res., 118, 1589-1603, DOI: 10.1002/jgra.50115, 2013.

# RECENT RESEARCH ACTIVITIES

## Microwave Heating of Various Carbon Powder by using Spatially Separated Magnetic Fields [1]

**(Laboratory of Applied Radio Engineering for Humanosphere, RISH, Kyoto University)**

Keiichiro Kashimura, Tomohiko Mitani and Naoki Shinohara

We experimentally investigated the microwave heating characteristics of non-magnetic conductive multi-particle systems using spatially separated electric and magnetic fields to determine the effects of the multi-particle structure on microwave heating. Pure carbon, carbon black, and artificial graphite multi-particle systems exhibited peak microwave absorption at specific relative densities under magnetic field rather than electric field. These absorptions can be categorized into two types: one originates from coupling between metal spheres, while the other originates from a heterogeneous distribution of particles.

Figure 1 shows the relative density dependence of the heating rates for various pure powder compacts subjected to E (Figure 1(a)) and H (Figure 1(b)) fields, respectively, when they were irradiated with 2.45GHz microwave whose maximum output was 1.5 kW. The pure carbon powder with a particle diameter of 20 μm has an electrical conductivity of 1 ~ 0.58 x$10^5$ S/m and can thus be regarded as a quasi-metal. Under magnetic field, a peak occurred in the heating rate for a relative density of 0.4205, corresponding to a maximum absorption of microwave power. For artificial graphite with a particle diameter of 80 μm (electrical conductivity: 5 ~ 2.4 x $10^3$ S/m), a similar tendency was observed. These compacts show a dramatic resonance at low relative densities (pure carbon: 0.3133; artificial graphite: 0.2225). This resonance has been reliably observed for both the heating rate and the maximum temperature. In contrast, under electric field, no such maximum absorption peak was observed for any of the carbon particles. Instead, the absorption decreased with increasing relative density.

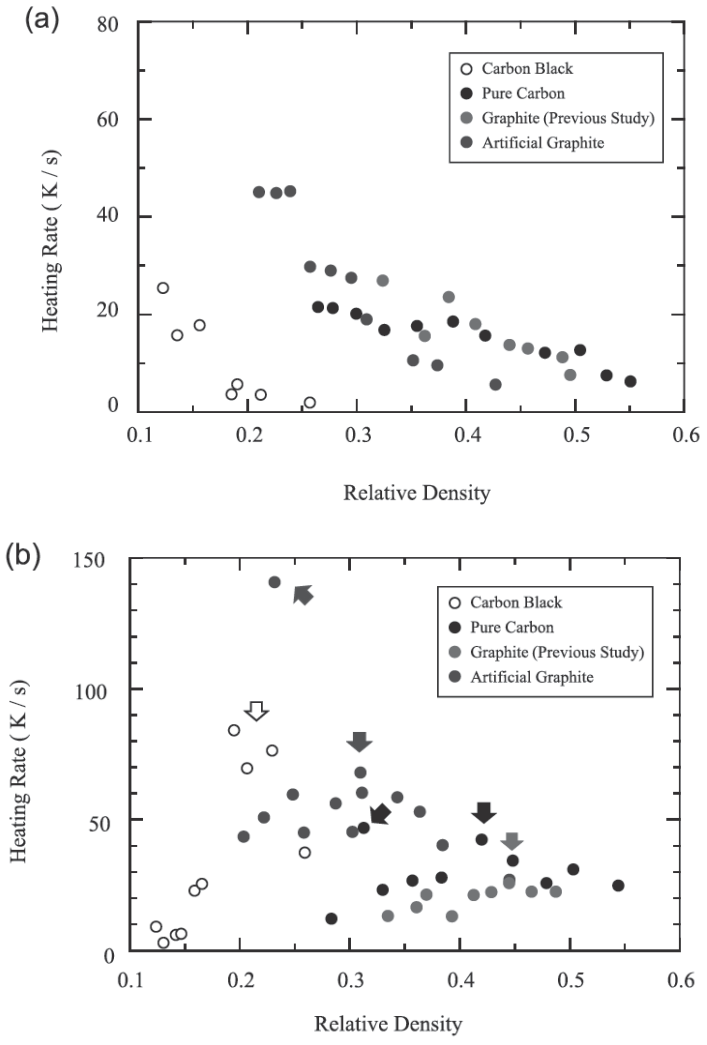


Figure 1. Relative density dependence of heating rates for various carbon powders compacts in (a) E and (b) H fields [1].

### References

[1] Kashimura, K., Hasegawa, N., Suzuki, S., Hayashi, M., Mitani, T., Shinohara N., Nagata, K., "Effects of relative density on microwave heating of various carbon powder compacts microwave-metallic multi-particle coupling using spatially separated magnetic fields", Journal of Applied Physics, vol.113, no.2, pp.024902-1-024902-5, 2013.

# RECENT RESEARCH ACTIVITIES

## Novel Space Environment Monitor, Instrument, and Space Mission Concepts

**(Laboratory of Space Systems and Astronautics, RISH, Kyoto University)**

Hiroshi Yamakawa, Hirotsugu Kojima, and Yoshikatsu Ueda

### Lorentz Force Spacecraft Formation Dynamics

Dynamics and control aspects of a charged satellite using the Lorentz force were investigated. The concept of the Lorentz-augmented charged satellite realizes propellant-less electromagnetic propulsion, using the interaction between an electro-statically charged satellite and the Earth's magnetic field. Charging of satellites can be controlled by devices like ion or electron gun. The devices are smaller and lighter than conventional chemical thrusters and suitable to be carried by small-size satellites. We investigated relative dynamics of two satellites orbiting around the Earth. One is a non-charged satellite called a target satellite, and the other is a charged satellite located near the target satellite on a circular orbit. We studied the effect of the Lorentz force on the relative motion of the chaser satellite with respect to the target satellite on an elliptic orbit or on a circular orbit as a special case.

#### Magneto-Plasma Sail (MPS) Space Propulsion System

An MPS (Magneto-Plasma Sail) is a unique propulsion system, which travels through interplanetary space by capturing the energy of the solar wind, which inflates a weak original magnetic field made by a super-conducting coil of about 2-10 m in diameter with an assistance of a high-density plasma jet. From our theoretical estimations, momentum transfer from the solar wind to a spacecraft with a coil is large enough if the plasma source is operated to inflate only the magnetic field away from the spacecraft. Our activities in 2006 are as follows: (a) Sizing (mass, dimension, current, etc.) of the super-conducting coil to produce magnetic field around the spacecraft, (b) Preparation of the experiment facility to measure magnetic field, temperature, current etc. around super-conducting coil.

### Miniaturization of plasma wave receiver system

To meet the recent requirements on the size, mass and power budgets in constellation missions or planetary missions, the miniaturization of plasma wave receiver is inevitable. The attempt to realize the extremely miniaturized plasma wave receiver have been made using analogue ASIC technology in the lab. The main activity in 2013 is the success in the development of the tiny waveform capture receiver, which is one of the typical types of plasma wave receivers. The size of the developed tiny waveform receiver is about one tenth of the conventional waveform receiver. Moreover, we also succeeded in implementing the preamplifier and the calibration system on the same analogue chip of the waveform receiver.

### Quantitative evaluation of electrochemical properties of fine-bubbles in water based on the type of gas

Recently, fine bubble (FB) hasfound applications in various fields. We have reported the effectiveness of water containing FB water of approximately 100 nm diameter for removal of radioactive cesium from soil and gravel conglomerate and nonwoven cotton. In Fukushima, this method of radioactive contamination removal using FB water is currently under trial. We also investigated the freshness-keeping effect of water containing FB on cut flowers such as a gentian, a lisianthus, and a small chrysanthemum. Although there were statistical dispersions in experimental results, FB was effective in keeping the freshness in the experiments. We focused our attention on the electrochemical properties of pure water (such as pH and electrical conductance) containing FB; we evaluated their correlation with the concentration of FB and investigated their potential for use as parameters for the characterization of FB in water.

Notes

# Devising a Framework for Holistic Development of the Natural Capital in Africa using GIS and Remote Sensing Techniques

SANGA-NGOIE Kazadi
Laboratory of Climate and Ecosystems Dynamics
Research Institute for Sustainable Humanosphere, Kyoto University, Kyoto, Japan

**ABSTRACT**

A scheme is devised in an attempt to assess the natural environmental capital (resources and services) of the African continent using GIS (Geographical Information Systems) and remote sensing techniques, in order to pave the way for a sustainable development of these environmental resources, while ensuring at the same time a continuous flow of materials and continuous metabolism all over the continent humanosphere. This scheme highlights the various development schemes best fitted to each one of the main African biomes. Specific environmental management procedures are recommended, and the renewable energy source with the most potentiality is specified, in order to reduce $CO_2$ emissions and to enhance $CO_2$ sequestrations over the continent.

## 1. INTRODUCTION

Africa is witnessing the coming of a new era of steady development aligned along the recent changes in the international geopolitics. However so far, Africa has been the object of many extraverted development schemes, most of them being hardly economically, socially and ecologically viable for the continent as a whole in the long term.

In fact, for these development schemes to be bear fruits and to be sustainable, we think that they have to be based on a new paradigm that should avoid as much as possible the blind copy of old models followed so far in most of the developed or developing countries. Most of these schemes have been characterized by large-scale environmental destruction, huge industrial wastes outpours and wide-spread pollutions of the air, water bodies and soils, for the sake of measurable economic development indicators alone (Miller, 2007; Chiraz, 2010).

The impacts of these changes, especially in terms of land development (human settlements, urban sprawl, slash and burn agriculture, fuel wood, bush fires, etc.), have been noted in the Congo River Basin, and are known to be part of a complex and ever-amplifying feedback cycle with global and regional climatic change as background (Sanga-Ngoie and Fukuyama, 1996).

Being nowadays the least advanced among the continents, Africa has nonetheless most of the assets it needs to fully and immediately embrace this approach to sustainable development. This can be especially possible if ways and means are devised so as (1) to monitor and assess, to protect, use and manage in an integrated and sustainable way, the African rich environmental capital and natural resources, and (2) to develop and use environment-friendly non-fossil energy resources with priority to integrating the economically-viable energy resources found within the continental perimeter. In other terms, African sustainable development has to be based on a thorough monitoring and consideration of its environmental and anthropogenic metabolism (Baccini and Brunner, 2012) as well as its capacity for integrated regional material flow (Brunner and Rechberger, 2004).

## 2. OBJECTIVES OF THE STUDY

In this note, we aim at assessing the potentials of the main environmental renewable resources in the African biomes. In our attempt to devise a scheme for sound and sustainable development at the continental scale, and from within the continent, we will mainly focus (1) on the relative natural capital that can be obtained from each one of these biomes, (2) on the overall availability of renewable energies in Africa, and (3) on the use of GIS and remote sensing techniques as the crucial instruments for data collection and integration both at the continental and the regional scales.

## 3. DATA SETS AND ANALYTICAL METHODOLOGY

In a previous study (Nonomura et al., 2003) using GIS techniques and remote sensing NOAA/AVHRR data (1985-1991), we obtained a digital vegetation model (DVM) map of the African continent based on Principal Components Analysis (PCA)

## Notes

of the NOAA channels 1, 2, 4 and 5 data. We foresee that this African land use/land cover map (Fig. 1) obtained for the early 1990s, hereafter the *Digital Vegetation Model (DVM),* will serve as the reference database to which more recent maps obtained by analyzing later ages data will be compared to for any change analysis over the continent.

Then, noting that over this continent well-positioned on both sides of the equator, rainfall is the main limiting factor when one wants to secure a stable biomass (food and biofuels) production, a precise knowledge of rainfall amounts at every location of the continent is necessary (Mberego and Sanga-Ngoie, 2014). It is notorious that rainfall data records on the African continent are very often non continuous and obtained at largely dispersed stations. For this, we opted to create a digital rainfall map of Africa using the following steps: (1) Normalized Difference Vegetation Index (NDVI) and Precipitable Water Index (PWI) are calculated from channels 1 and 2, and from channels 4 and 5, respectively; (2) Regression analysis using the 1st PCA component of monthly mean NDVI and PWI (as X), and the contemporaneous monthly mean rainfall data of observational stations (as Y) is performed to fit a second order quadratic function; (3) After validation, the obtained regression equations are used to produce the digital images of monthly rainfall for all the continent.

### 4. RESULTS

The African DVM so obtained shows that seven main land cover types (biomes) prevail on the continent (Fig. 1), and the coverage areas of each one of them are estimated. Moreover, monthly rainfalls are calculated, and the values for typical months of the year are shown in Fig. 2, illustrating the annual seasonal changes in rainy and dry seasons over the continent. From these analyses, the following findings have been highlighted.

#### *4.1 African climatic features*

The features of African rainfall seasonality is illustrated by the change in location of the rainy areas following the annual changes in the position of the sun over the continent: dry season prevails over those areas with less than 50 mm of monthly rains, while rainy season covers those areas with more than 50 mm of monthly rains. This north-south annual migration of the zone of heavy rains also highlights the deep relationship between rainfall and the position of the Inter-Tropical Convergence Zone (ITCZ), over the continent.

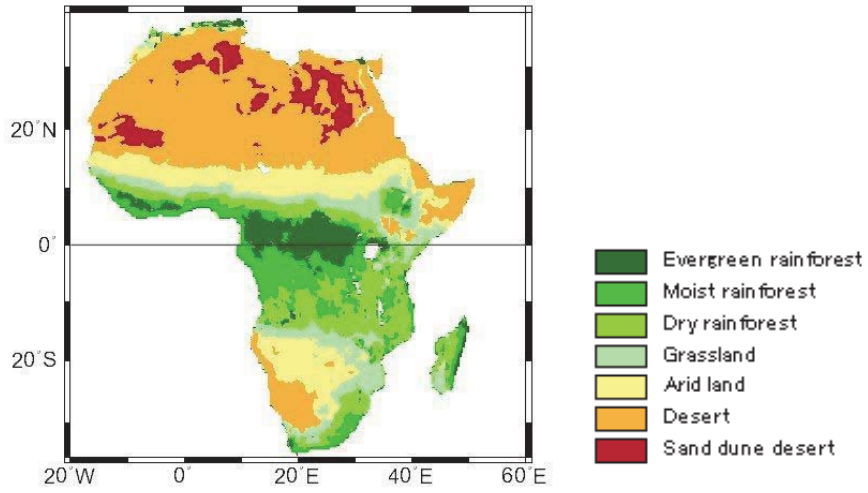


Fig. 1: The African Digital Vegetation Model (DVM)

#### *4.2 Ecozones and Biomes in the African Biosphere*

A combined evaluation of the African DVM and the regional climatic features shows that (Table 1):

(1) Out of the 30,307,000km$^2$ of its total area, the African continent includes the following ecozones (biomes): Evergreen Rainforests (*Erf*: 6.6%), Moist Rainforests (*Mrf*: 10.6%), Dry Rainforests and Savanna Woodlands (*Drf:* 14.7%), and

## Notes

Grasslands (*Grl*: 10.0%), Arid lands (*Arl*: 15.3%) and 42.8% of Deserts *Drt*) with large areas of Sand Dunes Deserts.

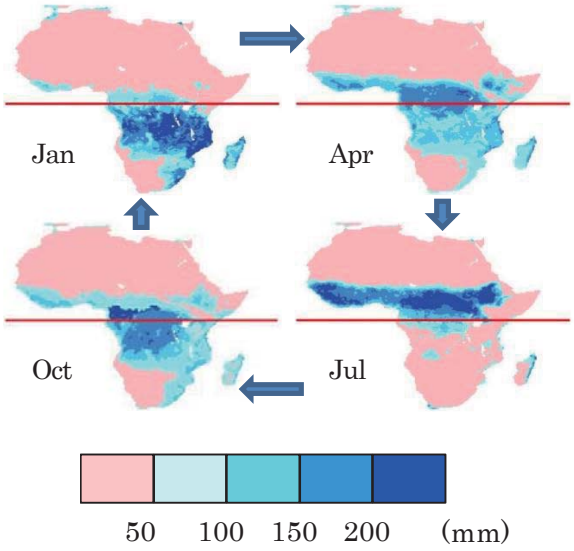


Fig. 2: Calculated African rainfalls for representative months: January, April, July, and October.

**Table 1: Africa's main ecozones (biomes).**

| LU/LC Types | Area ($10^6$km$^2$) | Area (%) | Main Countries |
|---|---|---|---|
| ***Erf*** | 2,006 | 6.6 | *DRC, Cameroon, Congo, Gabon |
| ***Mrf*** | 3.217 | 10.6 | DRC, Angola, Tanzania, Congo, Cameroon |
| ***Drf*** | 4.441 | 14.7 | DRC, Angola, Tanzania, Zambia, Mozambique |
| ***Grl*** | 3.031 | 10.0 | South Africa, South Sudan, DRC, Ethiopia |
| ***Arl*** | 4.656 | 15.3 | Sudan, Botswana, Nigeria, |
| ***Drt*** | 12.956 | 42.8 | Libya, Egypt, Algeria, Sudan |
| **Total** | **30.307** | **100.0** | |

*DRC: Democratic Republic of Congo)

(2) In general, *Erf* and *Mrf* are found in areas with 0-2 months of dry season, while *Drf* and *Grl* prevail in drier regions with up to 8 months of dry season. *Arl* and *Drt* are characterized by almost no rains (more than 9 months of dry season).

(3) Altogether, this information about the African land cover can be summed up into four main ecosystems with specific characteristics that have to be considered when development activities are concerned: **wet forests** (*Erl* and *Mrl*) covering 17.2% (5,220,000km$^2$) of African lands, **Savanna Woodlands** (*Drf*) covering 14.7% (4,441,000 km$^2$), **Grasslands** covering 10.0% (3,031,000km$^2$) of the lands, and **Arid** and **Desert lands** (*Arl* and *Drt*) spreading over 58.1% (17,613,000km$^2$) of the

continent (Fig.1, Table 1, see details in Nonomura et al., 2013).

It has to be noted here that Africa has relatively small tropical rainforest coverages compared to other tropical landmasses (Central and South Americas, Southern and Southeastern Asia), while having the largest extents of grasslands and deserts (Miller, 2007). On the other side, African forests are mostly primary and virgin forests biomes (therefore, a very rich biodiversity) in comparison to mostly secondary or planted mono-cultural forests in the developed countries (Western Europe, Northern America). All these African biomes, known to be very fragile, are in strong need for conservation and protection, instead of random development and destruction as done so far.

## 5. POTENTIAL SCHEMES FOR SUSTAINABLE RESOURCES MANAGEMENT

From the above-mentioned findings, it becomes clear that, in its search for sustainable and balanced development, Africa has a lot to gain by wisely taping in its huge environmental capital embedded in each one of its biomes, and on its untapped reserves of non-exhaustible renewable energy resources. At the same time, special attention has to be given for the restoration and preservation of those areas with fragile or unique ecosystems such as the deserts (*Drt*), arid lands (*Arl*) and the rainforests (*Erf, Mrf, Drf*) (Table 2).

**Table 2: Potential schemes for sustainable development for Africa**

- **Deserts (*Drt*)** :
  - Solar energy
  - Wind energy
- **Arid & Semi-arid Lands (*Arl*)**:
  - conservation
  - land restoration
- **Grasslands (*Grl*):**
  - agriculture
  - ranching , cattle
  - biomass, biofuels
  - industrial tree planting
  - afforestation
- **Dry Rainforests (*Drf*):**
  - conservation
  - reforestation, afforestation
- **Tropical Rainforests (*Erf* & *Mrf*)**:
  - air quality ($CO_2$)
  - $CO_2$ sequestration
  - biodiversity, conservation
- **Rivers and Lakes**:
  - water resources, biotopes
  - hydro-electricity

An astounding amount of $24{,}141\times10^{15}$W (1,366 W/m$^2$×17,613×109 m$^2$) of solar energy resource is reaching the African deserts surface (*Drt*) every second, while billions of megawatts of hydro-electricity power are there to be harnessed on daily basis from the main African Rivers (Congo, Niger, Zambeze, etc.) and their main tributaries flowing throughout the wet tropical rainforests (*Erf, Mrf*) area. Moreover, contrarily to Brazil and Indonesia where land development is almost impossible without systematic destruction of tropical rainforests (Yoshikawa and Sanga-Ngoie, 2011), agricultural development, for both food and renewable biofuels, can be developed on large-scales over African wet grasslands (*Grl*: 10.0%; 3,031,000km$^2$), as well as on selected areas of the dry rainforests (*Drf*), while, at the same time, protection of biodiversity will be the main rule in the lush rainforests (*Erf, Mrf*). Tree planting for reforestation or for industrial use (lumber, paper) could be developed over the *Drf* areas,

while systematic vegetation cover restoration plans have to be implemented for the climate-sensitive arid lands (*Arl*) areas.

## 6. CONCLUSION

Africa is known for its very poor and inconsistent atmospheric and climatological observational networks. Nowadays, remote sensing techniques are playing a very important role in providing reliable land cover data for every single place over this vast and very sparsely populated continent.

The fusion of these data together with available surface and statistical data on a GIS analytical platform has shown here that they can provide a sound basis for monitoring, assessing and planning for sustainable development of resources, especially the renewable ones, as well as for the restoration and conservation of African ecosystems for an endless flow of materials and continuous anthropogenic metabolism of this continent.

Scaling down the finding from the DVM to regional or local levels, using remote sensing data of appropriate time, spectral and spatial resolutions will make it possible to find out specific potentials and limitations at the country or area levels. If performed, these detailed quantitative assessments of the existing potentials for environmental land resources development and renewable energy generations, including solar, wind, bio- and hydro- energies, will pave the way to devising an integrated framework on the continental scale in terms of sustainable management, production and distribution. We think this integrated continental approach should be prioritized instead of the national schemes developed so far.

The DVM, the derived rainfall maps, as well as many other derivatives that can be obtained based on bio-physical or statistical relationships among observed parameters, could be the basis for re-defining new climatic maps as well as new *agro-ecological zones* (AEZ) using GIS and remote sensing techniques, which are shown here to be the right tools and techniques for sound decision-making aiming at appropriate action for sustainable development in Africa.

The scheme developed here is expected to contribute to both of the following: (1) reducing $CO_2$ emissions, especially those from fossil fuels, from the African continent, and (2) enhancing $CO_2$ sequestration by African forests (Sanga-Ngoie et al., 2012), and (3) supporting action for sustainable use and management of African ecological resources and its immense natural capital.

**Acknowledgement**

This notes is based on the contents of our presentation at the 2014 Symposium of the Kyushu Section of the Japan Remote Sensing Society, held at Saga University, Saga City, Japan on 2014.1.26. With all our deepest gratitude for been given this great scientific opportunity.

**References**

Baccini, P. and P.H. Brunner. Metabolism of the Anthroposphere, 2nd Edition. The MIT Press, Cambridge, Massachusets, USA. pp.392, 2012

Brunner, P.H. and H. Rechberger. Practical Handbook of Material Flow Analysis. Lewis Publ. London, UK. pp318, 2004.

Chiraz, D. D., Environmental Science 8th Edition, Jones & Barlett Publishers, Sudburry, 2010.

Mberego, S. and Sanga-Ngoie K. Using locally captured climate information for guiding local- level agriculturalists in Africa: a case study of Makonde District in Zimbabwe. *Jl. of Land Use Sci*. **9(2)**, 178-194, 2014.

Miller Jr., G.T., Environmental Science. 11th Edition. Thomson Brook/Cole, Belmont (2007).

Nonomura, A., Sanga-Ngoie K. and K. Fukuyama. Devising a new Digital Vegetation Model for Eco-climatic Analysis in Africa using GIS and NOAA/AVHRR Data. *Int. Jl. of Rem. Sens.* **24**, 3611-3633, 2003.

Sanga-Ngoie K. and K. Fukuyama. Interannual and long-term climate variability over the Zaire River Basin during the last 30 years. *JGR* **101 (D16)**, 21351-21360, 1996.

Sanga-Ngoie K., K. Iizuka and K. Kobayashi. Estimating $CO_2$ Sequestration by Forests in Oita Prefecture, Japan, by Combining LANDSAT ETM+ and ALOS Satellite Remote Sensing Data. *Remote Sens*. **4**, 3544-3570, 2012.

Yoshikawa, S. and Sanga-Ngoie K. Deforestation Dynamics in Mato Grosso in the Southern Brazilian Amazon using GIS and NOAA/AVHRR Data. *Int. Jl. of Rem. Sens*. **32(2)**, 523-544, 2011.

# ABSTRACTS (PH D THESIS)

## Anatomical and Mechanical Features of Palm Fibrovascular Bundles

**(Graduate School of Agriculture,
Laboratory of Biomass Morphogenesis and Information, RISH, Kyoto University)**

Shengcheng ZHAI

The palm family (Arecaceae, Palmae) consists of approximately 184 genera and 2400 species, is an important family of moncotyledon and palm plays an essential role in daily life of millions of people in tropical and subtropical regions. The properties and commercial utilization of palms are influenced by its structural characters. Until now researchers put most of their attention on the structural biology of commercial palms and there are many publications on oil palm (*Elaeis guineensis*) and coconut palms (*Cocos nucifera*). Tomlinson *et al*. [1, 2] did great research on the stem anatomy of palms. However, the anatomical and mechanical properties of fibrovascular bundles from leaf-sheath of palms, specially the palms widely distribute over the world, has not been studied well. In this thesis, the anatomical characteristics, mechanical properties and their functional implications were presented. This whole set of knowledge in palm leaf-sheath fibrovascular bundles could facilitate further understanding of archeological palm fiber-based products and utilization of these widespread natural fiber resources in future.

### Cell wall characterization of leaf fibers in palm and its functional implications [3]

The fibrovascular bundles from the lignified leaf sheath of windmill palm (*Trachycarpus fortunei*) are widely used as natural fibers for various products, and exhibit excellent durability. In this study, the cell wall of windmill palm fibers was characterized using transmission electron microscopy (TEM, 2000EX II, JEOL Co. Ltd, Tokyo, Japan), high resolution field emission scanning electron microscopy (FE-SEM, JSM-6700F, JEOL Co. Ltd, Tokyo, Japan), and polarized light microscopy (PLM), and chemical analysis to measure lignin content. It was found that (1) the secondary wall was composed of just two layers (Fig. 1), outer (equivalent to $S_1$, 0.65±0.12 μm) and inner (equivalent to $S_2$, 1.28±0.30 μm) ones, with a high ratio of $S_1$ to the whole cell wall thickness; (2) the microfibrils of the $S_1$ are orientated in an S-helix (MFA, 127.0°±2.0), and those of the $S_2$ in a Z-helix (MFA, 43.7°±2.2); and (3) the Klason lignin content of fiber bundles was very high (nearly 40%). It is suggested that these structural and chemical features of windmill palm fibers are involved in their mechanical properties such as high flexibility and elasticity, and also related to their high durability.

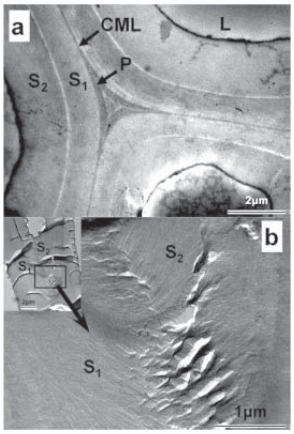


Figure 1. Electron micrographs of the windmill palm fiber. – a: Transverse section clearly shows a two-layered structure of the secondary wall. CML: compound middle lamella; L: lumen; P: primary wall; S1, S2: outer and inner layers of the secondary wall. – b: Enlargement of the fiber tip in oblique section, demonstrating microfibril orientation in the two layers of the secondary wall [3].

The cell wall organization of leaf sheath fibers in different palm species was also studied with PLM and TEM. The secondary wall of the fibers consisted of only two layers, $S_1$ and $S_2$. The thickness of the $S_1$ layer in leaf sheath fibers from the different palm species ranged from 0.31 to 0.90 μm, with a mean value of 0.57 μm, which was thicker than that of tracheids and fibers in secondary xylem of conifers and dicotyledons. The thickness of the $S_2$ layer ranged from 0.44 to 3.43 μm, with a mean value of 1.86 μm. The ratio of $S_1$ thickness to the whole cell wall thickness in palm fibers appears to be higher than in secondary xylem fibers and tracheids. We suggest that the two-layered structure in the secondary wall of palm leaf fibers, which presumably also applies to the homologous fibers in palm stems, is a specific character different from the fibers in other monocotyledons (such as bamboo and rattan) and dicot wood [4].

# ABSTRACTS (PH D THESIS)

**Mechanical characteristic of fibrovascular bundles among different genus in palm and its structural implications**

This thesis also presented mechanical properties, microfibril angles (MFAs) and Klason lignin contents of leaf sheath fibrovascular bundles from 14 palm genera.

Observed by light microscopy, all fibrovascular bundles consisted equally of thick-walled sclerenchyma fibers and vascular tissue, while the shape and localization of vascular tissues on the transverse sections varied among species. It was possible to group these fibrovascular bundles into 3 types based on the vascular tissue's differences[5]: type A – rounded in the central region; type B – angular in the marginal region; and type C – aliform in the central region (Fig. 2). These three anatomical types of fibrovascular bundles showed some correlation with a current phylogenetic classification of palm species. Through mechanical tests, this research confirmed the correlation between diameter and mechanical properties of the fibrovascular bundles of palms; tensile strength and Young's modulus showed a decreasing trend with increasing diameter. We clarified that this trend was due to a marked increase in the proportion of transverse sectional area comprised by vascular tissue with increasing diameter of fibrovascular bundles. The MFAs of fibrovascular bundles ranged from 10.3º to 47.1º, which were generally larger than those of non-woody plants, conifers, and broad-leaved trees. The Klason lignin contents of palm species were also high, ranging from 18.3% to 37.8%, with a mean value of 29.6%. These large MFAs and high lignin contents could lead to the long-term plastic deformation and relatively low tensile strength of palm fibrovascular bundles. The observed MFA features might also have a relationship with the biomechanical movements of fiber bundles in the windmill palm[7].

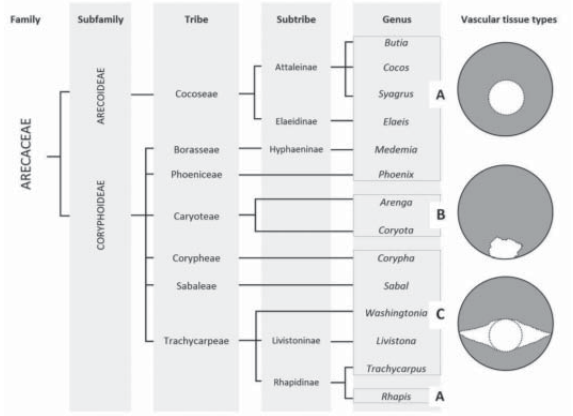


Figure 2. A diagram to show the phylogenetic classification of 14 genera of palms (Arecaceae), redrawn from Dransfield *et al*. [6] and Tomlinson *et al*.[2]. A, B, C indicate the three types of vascular tissues in fibrovascular bundles, where the gray area is occupied by sclerenchyma fibers and the white area by a vascular tissue.

**Acknowledgements**

The author thanks Prof. Keiji Takabe, Hiroyuki Yano, Kenji Umemura, Tuyoshi Yoshimura, Bunzo Mikami, Kentaro Abe, Aya Yanagawa for helping to carry out different experiments in their labs, Kyoto University. Also there are many thanks to Dr. Yoshiki Horikawa, Misao Yokoyama and Rie Endo for the resin embedding method and TEM observation. This research was supported by the G30 Program of the Faculty of Agriculture, Kyoto University, and the Kambayashi Scholarship Funding.

**References**

[1] Tomlinson, P.B. The structural biology of palms. Clarendon Press, Oxford, 1990.

[2] Tomlinson, P.B., Horn, J.W., Fisher, J.B. The anatomy of palms. Oxford University press, New York, 2011.

[3] Zhai, S., Horikawa, Y., Imai, T. and Sugiyama, J. Cell wall characterization of windmill palm (*Trachycarpus fortunei*) fibers and its functional implications. *IAWA Journal*, 34(1): 20-33, 2013.

[4] Zhai, S., Horikawa, Y., Imai, T. and Sugiyama, J. Cell wall ultrastructure of palm leaf fibers. *IAWA Journal*, 35(2): 127-137, 2014.

[5] Zhai, S., Horikawa, Y., Imai, T. and Sugiyama, J. Anatomical and mechanical characteristics of leaf-sheath fibrovascular bundles in palms. *IAWA Journal*, 34(3): 285-300, 2013.

[6] Dransfield, J., Uhl, N.W., Asmussen, C.B, Baker, W.J., Harley, M.M. and Lewis, C.E. Genera Palmarum. The evolution and classification of palms. Kew Publ., Royal Botanic Garden, Kew, 2008.

[7] Zhai, S., Li, D., Pan, B., Sugiyama, J. and Itoh, T. Tensile strength of windmill palm (*Trachycarpus fortunei*) fiber bundles and its structural implications. *Journal of Material Science*, 47: 949-959, 2012.

# ABSTRACTS (PH D THESIS)

## Functional characterization of a RING-type ubiquitin ligase and MYB transcription factors involved in secondary cell wall formation

**(Graduate School of Agriculture,
Laboratory of Metabolic Science of Forest Plants and Microorganisms,
RISH, Kyoto University)**

Soichiro Noda

Lignified secondary cell walls are formed in sclerenchymatous cells such as vessel elements, tracheids, and fibers. In lignified secondary walls, regularly arranged and rigid cellulose microfibrils are coated with hemicelluloses, and the gap is filled with lignin. Deposition of lignified secondary walls gives high mechanical strength to sclerenchymatous cells and enables them to support plant bodies and to resist negative pressure caused by water transportation. Recently, many transcription factors which coordinately regulate biosynthesis of the secondary wall components have been uncovered in a model dicotyledonous plant *Arabidopsis thaliana*. However, little was known about other regulatory systems of secondary wall formation. In addition, the transcriptional regulation of secondary wall formation in Gramineae plants, which have cell wall compositions different from those of dicotyledonous plants, is not known well. In the present study, the author indicated that an E3 ubiquitin ligase, which plays an important role in the selective protein degradation via the ubiquitin-proteasome pathway, was involved in secondary wall formation. Furthermore, novel rice MYB transcription factors involved in secondary wall formation were characterized.

First, the author conducted a gene co-expression network analysis and found that *Arabidopsis Tóxicos en Levadura54* (*ATL54*, At1g72220) encoding a putative ubiquitin ligase was co-expressed with some genes involved in secondary wall formation. The recombinant ATL54 protein catalyzed E1- and E2-dependent auto-ubiquitination. Expression of some biosynthetic genes of secondary wall components was up-regulated in apical stem portions of the *ATL54*-knock-out mutants, while expression of a gene involved in programmed cell death of tracheary elements was significantly repressed in both *ATL54*-knock-out and *ATL54*-overexpressed mutants. These results suggested that ATL54 was an E3 ubiquitin ligase involved in secondary wall biosynthesis and programmed cell death during xylogenesis [1].

Second, the author showed that the *β-glucuronidase* (*GUS*) reporter gene driven by the *ATL54* promoter was significantly expressed in interfascicular fibers, xylary fibers, and vessels in inflorescence stems. The dual luciferase transient transfection assay demonstrated that *ATL54* was transactivated by MYB46, a master regulator of secondary wall biosynthetic genes. In addition, an electrophoretic mobility shift assay showed that MYB46 directly bound to *ATL54* promoter fragments. These results indicated that *ATL54* expression was directly regulated by MYB46 [2].

Third, using a gene co-expression analysis, six genes of MYB transcription factors were found to be co-expressed with cellulose, xylan, and lignin biosynthetic genes in rice (*Oryza sativa* cv. Nipponbare). A phylogenetic analysis of *Arabidopsis* and rice MYB transcription factors showed that the six MYB transcription factors shared similarities with *Arabidopsis* MYB transcription factors regulating secondary wall biosynthesis [3]. A quantitative real-time PCR analysis revealed that four *MYB* genes were highly expressed in culm internodes, culm nodes, hulls, or leaf sheaths of rice, where secondary wall develops well. The transcriptional activation activity of the MYB transcription factors showed that all the four MYB transcription factors can activate gene expression in yeast.

To identify downstream target genes of the MYB transcription factors, a dual luciferase transactivation assay was performed. A cellulose synthase gene required for secondary wall biosynthesis [4], *OsCesA7*, was transactivated by two MYB transcription factors. In addition, an electrophoretic mobility shift assay showed that one of the MYB transcription factors caused a band shift of oligonucleotides containing *cis*-elements within the *OsCesA7* promoter. These results indicated that *OsCesA7* was a direct downstream target of the MYB transcription factor.

Taken together, this study suggested that selective protein degradation via the ATL54-mediated ubiquitin-proteasome pathway may be involved in secondary wall formation. In addition, it also provided a deeper insight into transcriptional regulation of secondary wall biosynthesis in Gramineae.

# ABSTRACTS (PH D THESIS)

**Acknowledgements**

The author thanks Associate Professor Dr. Masatoshi Yamaguchi, Saitama University, Assistant Professor Dr. Koji Yamaguchi, Kinki University, and Professor Dr. Tsutomu Kawasaki, Kinki University for technical advice. The author also thanks Professor Dr. Taku Demura, Nara Institute for Science and Technology and Dr. Nobuyuki Nishikubo, Oji Paper Co., Ltd. for transgenic *Araidopsis* lines and helpful discussion. This research was performed as a collaborative program of Development and Assessment of Sustainable Humanosphere/Forest Biomass Analytical System (DASH/FBAS) of Research Institute for Sustainable Humanosphere (RISH), Kyoto University.

**References**

[1] Noda S, Takahashi Y, Tsurumaki Y, Yamamura M, Nishikubo N, Yamaguchi M, Sakurai N, Hattori T, Suzuki H, Demura T, Shibata D, Suzuki S, Umezawa T (2013) ATL54, a RING-H2 domain protein selected by a gene co-expression network analysis, is associated with secondary cell wall formation in *Arabidopsis*. *Plant Biotechnol* 30: 169–177

[2] Noda S, Yamaguchi M, Tsurumaki Y, Takahashi Y, Nishikubo N, Hattori T, Demura T, Suzuki S, Umezawa T (2013) ATL54, a ubiquitin ligase gene related to secondary cell wall formation, is transcriptionally regulated by MYB46. *Plant Biotechnol* 30: 503–509

[3] Zhong R, Lee C, Zhou J, McCarthy RL, Ye Z-H (2008) A battery of transcription factors involved in the regulation of secondary cell wall biosynthesis in *Arabidopsis*. *Plant Cell* 20: 2763–2782

[4] Tanaka K, Murata K, Yamazaki M, Onosato K, Miyao A, Hirochika H (2003) Three distinct rice cellulose synthase catalytic subunit genes required for cellulose synthesis in the secondary wall. *Plant Physiol* 133: 73–83

ABSTRACTS (PH D THESIS)

# Evaluation of Structural Performance of CLT Joint

**(Graduate School of Agriculture,
Laboratory of Structural Function, RISH, Kyoto University)**

Shoichi Nakashima

## Introduction

Cross Laminated Timber (CLT) is the structural timber panel for buildings. In the 90's, that is developed in Europe, and expected as a new material for the structural wall panel and/or floor in Japan. We chose the dowel type joint as the connectors to fix wall. The major benefits expected for CLT dowel type joints are the small dependence of load carrying capacity on angular orientation, and large deformation ability due to the prevention of failures along the laminae axis. The load carrying capacity of dowel type joints were evaluated by experiments, yield theory [1], and numerical to contribute to establish a design method of the joints.

## Non-linear Behavior of Single CLT Drift Pin Joint

Image of dowel type leg joints with the CLT panel were shown in Fig.1 (a)(b). Usually, the dependence on angular orientation evaluated by Hankinson's experimental equation [3] and behavior of bar on the timber expressed by Winkler's foundation model [2]. Therefore, we predict the load-deformation relationships of CLT drift pin joints using FEM analysis based on these two theories, and that were verified by experiments (Fig.2 (a)(b)).

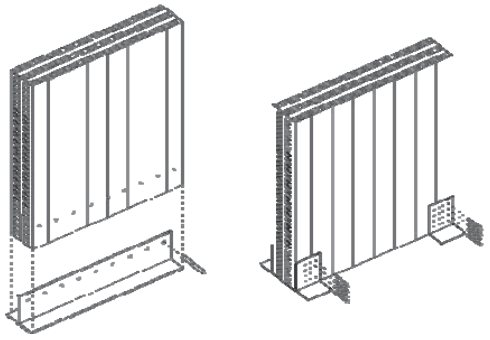

(a) CLT drift pin joint (b) CLT screw joint
Figure 1. Images of CLT dowel type joint.

Tensile test of single drift pin joint was performed for the verification. The test parameter was determined to the laminae axis orientation against the load direction (0°, 45°, and 90°) for clarity the variation of the load-deformation relationships. Those relationships were measured by setups shown in Figure 2(a). The small dependences of structural performance of drift pin on angular orientation were verified [4]. Also, the horizontal structural performance of CLT shear wall with drift pin joint was verified by FEM analysis and experiments [5].

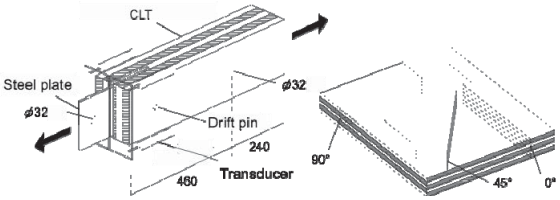


(a) Tensile test of single joint (b) Specimens
Figure 2.Experiment setup.

## Failure Behavior of Single CLT Drift Pin Joint

Figure 4, 5 and 6 show the test parameters for the consideration of the failure factor around the connection, failure figure and an example of the test result; relationship between failure load and effective shear area.

Sprit or shear failures along the axis direction of each lamina were expected on the test parameters figure 4, however, actual failures were shear failure around the border of layers and rolling shear and/or tensile failure of the perpendicular layers.

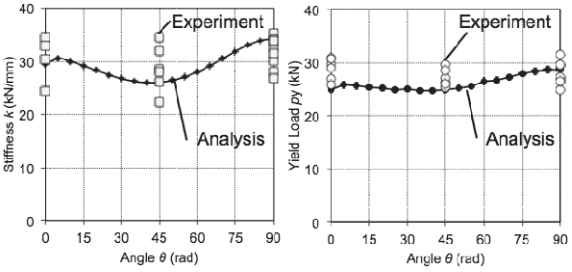


Figure 3. Effect of loading angle against the tensile performance of drift pin joint.

# ABSTRACTS (PH D THESIS)

The failures around the pin were not observed on the connection that has largest effective shear area ($e_1e_2$=7*7$d^2$). The maximum load and deformation were compared with logarithm of effective shear area. Logarithm was taken for the consideration of stress concentration around the hole.

**Deference between Single CLT Screw Joint and Single CLT Drift Pin Joint**

Same as CLT drift pin joint, CLT screw joint shown in figure 1(b) also was performed tensile test of single joint. The increase in the resistance load after the yielding by withdrawal resistance was observed on tensile test of single CLT screw joint. On the other hand, the joint has weakness against cyclic loading targeted in the positive and negative direction. Brittle failure arise from the material property of the screw was the caused of this phenomenon.

**Conclusion**

The merits of CLT dowel type joint are; (a) The small dependence on angular orientation caused of the cross lamination (b) The large ductility caused of the prevention of failures along the axis direction of each lamina. CLT screw joint resists against the tensile load by not only bending of the fastener but also withdrawal of the fastener.

**Acknowledgements**

This work was supported by Grant-in-Aid for JSPS Fellows, 2013.

**References**

[1] H.J. Blaß, T. Uibel, "Load Carrying Capacity of Joints with Dowel Type Fasteners in Solid Wood Panels", *CIB-W18*/39-7-5 2006

[2] Kuenzi E.W., "Theoretical Design of Nailed or Bolted Joint Under Lateral Load", *USDA*. No.D1951 1955.

[3] S.C. Cowin, "On the Strength Anisotropy of Bone and Wood", *J.App. Mechanics, Transaction of the ASME* Vol.46 832-838 1979.

[4] Shoichi Nakashima, "Propose Alternative Design Criteria for Dowel Type Joint with CLT", *Materials and Joints in Timber Structures, Recent Developments of Technology*, RILEM Bookseries Vol.9 39-748 2014

[4] Shoichi Nakashima, "Evaluation of Tensile Performance of Drift Pinned Joint with Steel Plate on Cross Laminated Timber", *J. Struct. Constr. Eng.,* Vol.78 No.687 969-975 2013.

[5] Shoichi Nakashima, Akihisa Kitamori,Zeli Que, Kenji Komatsu, Kohei Komatsu "Evaluation of In-Plane Shear Performance of Cross Laminated Timber Shear Wall with Drift Pinned Leg Joint", *J. Strct. Eng*. Vol.59B 529-536 2013

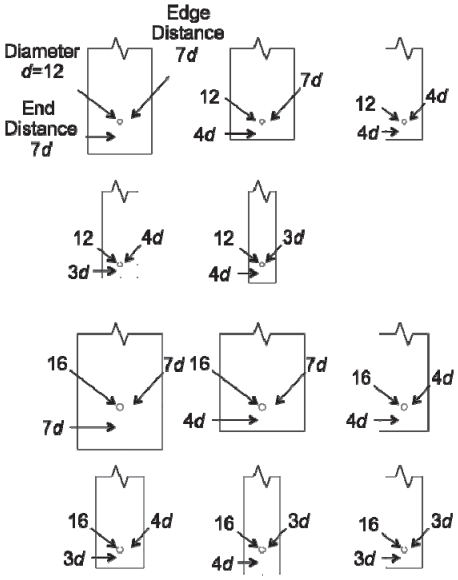


Figure 4. Test Parameters

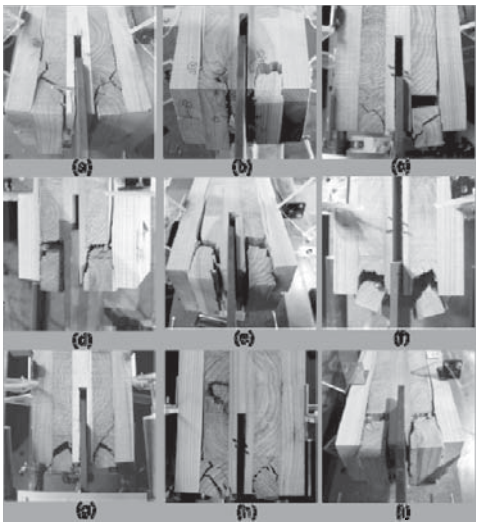

Figure 5. Shear failure on the border of the laminae.

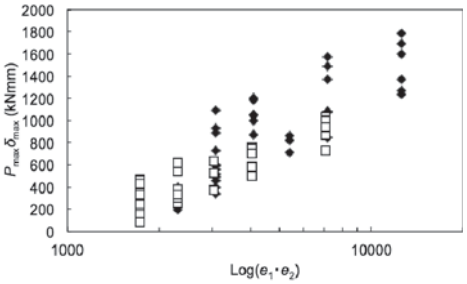


Figure 6. Maximum Load ($P_{max}$), Deformation ($\delta_{max}$) – Effective Shear Area ($e_1$ •$e_2$) Relationships of Drift Pinned Joint. Legends: □: Drift pin diameter $d$ =12, ◆: Drift pin diameter $d$ =16.

# ABSTRACTS (PH D THESIS)

## Study on Propulsive Characteristics of Magnetic Sail and Magneto Plasma Sail by Plasma Particle Simulations

**(Graduate School of Engineering,
Laboratory of Space Systems and Astronautics, RISH, Kyoto University)**

Yasumasa Ashida

Magnetic Sail is a spacecraft propulsion system that generates an artificial magnetosphere to block solar wind particles and uses the imparted momentum to accelerate a spacecraft (Figure 1). The derivative of Magnetic Sail, Magneto Plasma Sail inflate the artificial magnetosphere by a plasma injection from the spacecraft. The momentum caught by the inflated magnetosphere is transfer to the spacecraft as a larger thrust. However, the propulsive characteristics of magnetic sail and magneto plasma sail has not been quantified even thought the many previous works were carried out. This is because the large computational efforts is required to simulate the momentum transfer process including the plasma kinetics and the scaling law of the propulsive characteristics cannot be obtained under the one simulation model.

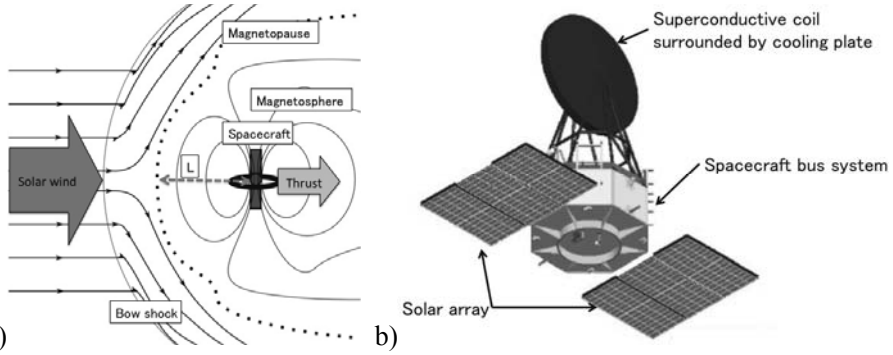


Figure 1 a) schematic illustration of Magnetic Sail and b) spacecraft model of Magneto Plasma Sail.

In the present study, the plasma flow around Magnetic Sail and Magneto Plasma Sail is simulated from the ion inertial scale, where ion Larmor motion is comparable with the artificial magnetosphere size, to the electron inertial scale, where electron Larmor radius and Debye length are comparable with the magnetosphere size. The steady-state model of plasma flow around magnetic sail including ion kinetic effects had to be developed by using Flux-Tube model to enable us to drastically shorten the simulation time required to reveal the propulsive characteristics with various parameters. Using the high performance computing techniques and the recently developed peta-scale supercomputer, the highly parallelized simulation code based on Full Particle-in-Cell (PIC) model was also developed to take the electron kinetic effects into consideration.

Three type of simulation: three-dimensional Flux-Tube model, two-dimensional Full-PIC model and three-dimensional Full-PIC model are hence performed to reveal scaling law of the propulsive characteristics of Magnetic Sail and Magneto Plasma Sail. The thrust of magnetic sail is approximately proportional to the magnetic moment of onboard superconductive coil on the electron inertial scale even though the thrust is approximately proportional to the 2/3 power of the magnetic moment on the ion inertial scale (Figure 2). The thrust changes from the electron inertial scale to the ion inertial scale nonlinearly. The empirical formula of thrust was obtained by the combination of Flux-Tube model and Full-PIC model. It was also revealed that these propulsive characteristics are caused by the finite Larmor motion and charge separation between ion and electron. The solar wind that is a natural phenomenon changes its parameters such as number density and velocity every moment. The propulsive characteristics about solar wind variation were also examined. The thrusts on the electron inertial scale and the ion inertial scale are proportional to the 1.15 power of number density and the 0.67 power of number density, respectively. This propulsive characteristics cause the difference in the flexibility of the interplanetary flight missions by magnetic sail since the average plasma density is inversely proportional to square of the sun-spacecraft

# ABSTRACTS (PH D THESIS)

distance. It was also revealed that the magnetic sail on the ion inertial scale, which thrust is inversely proportional to the 1.3 power of the sun-spacecraft distance is more suitable for the deep space flight than the magnetic sail on the election inertial scale, which thrust is inversely proportional to the 2.3 power of the sun-spacecraft distance.

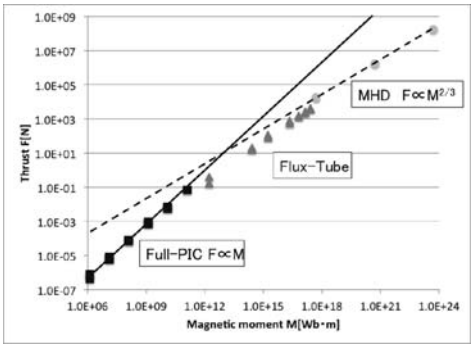


Figure 2 thrusts of magnetic sail with various magnetic moments.

Two- and three-dimensional simulations demonstrate the increase in thrust of Magneto Plasma Sail utilizing plasma injection. It becomes clear that the increase in thrust is dependent on the Larmor radius of injection plasma and the plasma energy at injection point. By simulations with various plasma parameters and one-dimensional theoretical analysis, we examined the parameters that maximize a thrust. The maximum increase (thrust of MPS / thrust of magnetic sail) is 97 but the thrust gain (thrust of MPS / (thrust of magnetic sail + thrust of plasma jet)) is only 0.4 by same condition. On the contrary, the maximum thrust gain 5.2 is obtained and the relation of trade-off between the increase in thrust and the thrust gain is revealed (Figure 3).

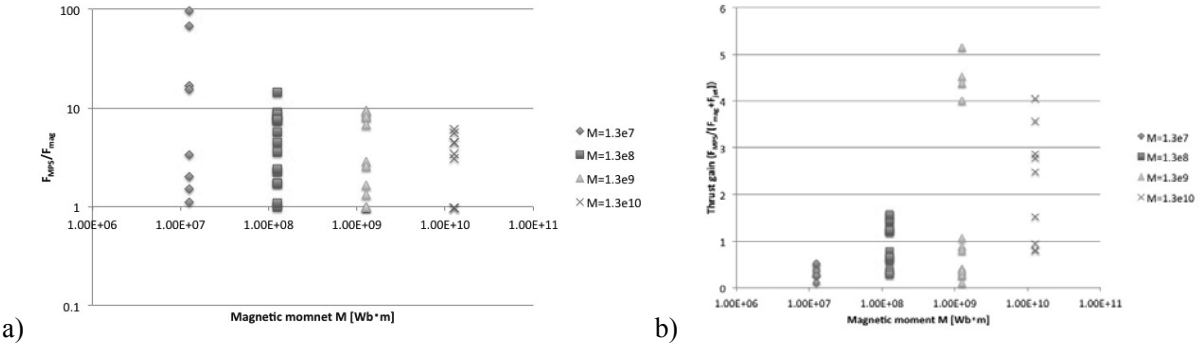


a) b)

Figure 3 a) thrust increase and b) thrust gain of Magneto Plasma Sail.

Moreover, the propulsive characteristics other than thrust: thrust-mass ratio, thrust-power ratio and specific impulse, were also examined. The thrust-mass ratio is approximately constant on the electron inertial scale and gradually decreases on the ion inertial scale as the magnetic moment of the onboard coil becomes large. The thrust-power ratio is mainly depends on the plasma injection velocity and, when the thrust gain is large the thrust-power ratio is also large. However, it was revealed that the high thrust-mass ratio, the high thrust-power ratio and specific impulse couldn't be achieved simultaneously. Under the limitation of the present technology and the propulsive characteristics, the feasible demonstration missions of Magnetic Sail and Magneto Plasma Sail are also proposed. The optimized trajectory obtained by Genetic Algorithm shows that large acceleration is obtained even the small-scale Magnetic Sail by the flight via an inner planet. The artificial halo orbit at Lagrange points are also proposed as the candidate of the magnetic sail mission.

Concluding the present thesis, the scaling law of the propulsive characteristics of Magnetic Sail and Magneto Plasma Sail are successfully revealed, with a few suggestions for realization of future interplanetary missions.

# ABSTRACTS (PH D THESIS)

## Characterization of *O*-methyltransferases involved in lignan biosynthesis

**(Graduate School of Agriculture, Department of Applied Life Sciences, Laboratory of Metabolic Science of Forest Plants and Microorganisms, RISH, Kyoto University)**

Safendrri Komara Ragamustari

Lignans are a group of phenolic compounds where two phenylpropanoid units are coupled by the central carbon (C8) of their side chains. These compounds have been gaining much interest due to their important biological activities, such as antitumor property, as well as unique stereochemical mechanisms for their biosynthesis. Albeit several reports on cDNAs encoding enzymes involved in lignan biosynthesis, little is known about *O*-methyltransferases (OMTs) in lignan biosynthesis (lignan OMTs), and no cDNAs encoding lignan OMTs have been isolated. In addition, nothing has been known about enzymes involved in the biosynthesis of phenylpropanoid monomers which are dedicated to the biosynthesis of lignans, but not lignins. In the present study, the author isolated and characterized cDNAs that encode lignan OMTs in relation to regio- and enantiomeric selectivities for the first time. The author also examined cinnamyl alcohol dehydrogenases (CADs) which are possibly involved in lignan biosynthesis.

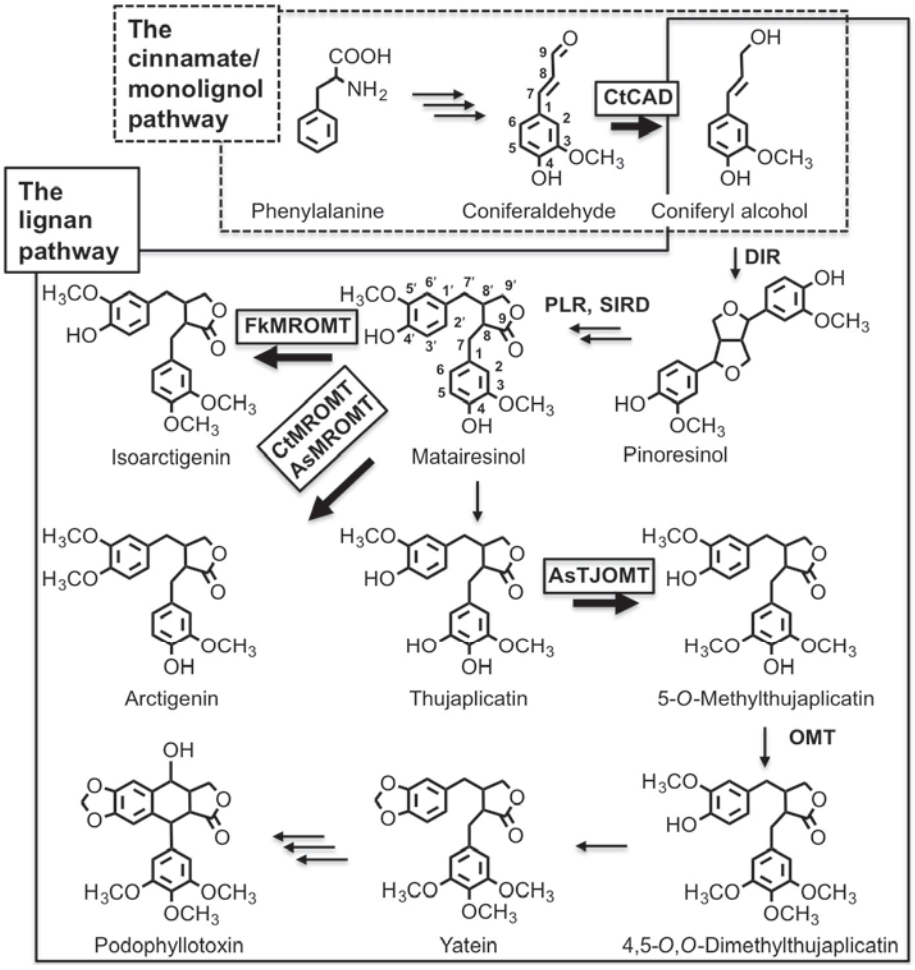


Figure. The cinnamate/monolignol and lignan biosynthetic pathways. DIR: dirigent protein, PLR: pinoresinol/lariciresinol reductase, SIRD: secoisolariciresinol dehydrogenase. Boxed: isolated/characterized in this study.

# ABSTRACTS (PH D THESIS)

First, a *Carthamus tinctorius* (safflower) cDNA encoding an OMT methylating a lignan was characterized for the first time. Its recombinant OMT catalyzed regioselective methylation of matairesinol to give rise to an antitumor lignan, arctigenin (4′-*O*-methylmatairesinol) (Figure), and designated as *C. tinctorius* matairesinol OMT (CtMROMT). Gene expression analysis and biochemical characterization of the OMT indicated that CtMROMT is responsible for arctigenin biosynthesis in *C. tinctorius*. In addition, two other cDNAs encoding matairesinol-methylating OMT, each from *Anthriscus sylvestris* (cow parsley) and *Forsythia koreana* (Korean forsythia), were isolated and designated as *AsMROMT* and *FkMROMT*, respectively. AsMROMT showed the same regioselectivity of matairesinol methylation as CtMROMT, whereas FkMROMT gave rise to only isoarctigenin, exhibiting the regioselectivity opposite to those of Ct and AsMROMTs (Figure).

Next, enantiomeric control of the three MROMTs was examined; all MROMTs exhibited strict enantioselectivity, giving rise to only (−)-enantiomers of their products. This is in sharp contrast to the previously proposed mechanism for matairesinol methylation by a *Forsythia intermedia* (golden bell) crude OMT preparation, which showed neither regioselectivity nor enantiomeric selectivity.

Third, a cDNA responsible for the first *O*-methylation step in the biosynthesis of podophyllotoxin (another antitumor lignan) from matairesinol (Figure) was isolated from *A. sylvestris*. The recombinant OMT catalyzed regioselective *O*-methylation of thujaplicatin to afford 5-*O*-methylthujaplicatin. Based on the gene-expression and biochemical analyses, it was concluded that this is the first example of a cDNA encoding an enzyme in the podophyllotoxin biosynthetic pathway from matairesinol, and was designated as thujaplicatin OMT (AsTJOMT).

In addition, characterization of CAD-encoding cDNAs was also conducted. CADs are responsible for the last reductive step in monolignol biosynthesis, which are precursors to lignin and lignans (Figure). Three *C. tinctorius* CADs were isolated and designated as *CtCAD1*, *CtCAD2* and *CtCAD3*. Gene expression analysis and biochemical characterization of plant and recombinant CADs suggested that CtCAD2 and CtCAD3 were involved in lignin and lignan biosynthesis, while CtCAD1 is most likely to be involved in plant defense mechanism.

**References**

[1] Umezawa, T., Ragamustari, S.K., Nakatsubo, T., Wada, S., Li, L., Yamamura, M., Sakakibara, N., Hattori, T., Suzuki, S., and Chiang, V.L., "A novel lignan *O*-methyltransferase catalyzing the regioselective methylation of matairesinol in *Carthamus tinctorius*," *Plant Biotech*, vol. 30, 97-109, 2013.

[2] Ragamustari, S.K., Shiraiwa, N., Hattori, T., Nakatsubo, T., Suzuki, S., and Umezawa, T., "Characterization of three cinnamyl alcohol dehydrogenases from *Carthamus tinctorius*," *Plant Biotech*, vol. 30, 315-326, 2013.

[3] Ragamustari, S.K., Nakatsubo, T., Hattori, T., Ono, E., Kitamura, Y., Suzuki, S., Yamamura, M., and Umezawa, T., "A novel *O*-methyltransferase involved in the first methylation step of yatein biosynthesis in *Anthriscus sylvestris*," *Plant Biotech*, vol. 30, 375-384, 2013.

[4] Ragamustari, S.K., Yamamura, M., Ono, E., Hattori, T., Suzuki, S., and Umezawa, T., "Substrate-enantiomer selectivity of matairesinol *O*-methyltransferases," *Plant Biotech*, in press.

# ABSTRACTS (MASTER THESIS)

## Investigation of wooden artifacts in Korea – durability of yellow heart pine and vessel arrangement in hardwood species used in woodblocks

**(Graduate School of Agriculture,
Laboratory of Biomass Morphogenesis and Information, RISH, Kyoto University)**

Lee Jihye

I conducted my study about historically and culturally important wooden artifacts in Korea. Firstly, biological durability of Yellow Heart Pine (Hwangjangmok) that has been long used in traditional imperial wooden constructions in Korea was investigated. Secondary, the development of non-destructive analytical methods to investigate wood properties of important cultural asset, in my case, Tripotaka Koreana, was conducted.

Hwangjangmok, *Pinus densiflora* for. *erecta* Uyeki was a kind of red pine[1)] that were often older than 100 years. It had relatively large reddish-brown heartwood, narrow and even annual-ring width. The termite test, white-rot fungi test and brown-rot fungi test were performed. However, to my surprise, there was no remarkable difference between normal red pine and Hwangjangmok.

Tripitaka Koreana, a 13$^{th}$ century edition of scriptures known to be the world's most comprehensive and oldest intact version of Buddhist scriptures, engraved on 81,340 wooden plates during Koryo Dynasty from 1236 to 1251 A.D. The printing woodblocks has been maintained over several centuries partly because the Haeinsa temple located away in a secluded valley in the deep mountains, and partly because the storage building of woodblocks was so well designed to keep them dry.

According to the latest survey from 244 wooden samples collected from Tripitaka Koreana, more than 62% of whole specimens investigated was *Prunus sp*., which were used in wooden plate 64%, and wooden plate edge 56%. *Pyrus sp*. was used 13% of whole specimens and 31% of wooden plates. Therefore, 75% of whole Tripitaka Koreana was made by these two species. As minor selections, *Acer sp*., *Betula sp*., *Machilus* sp., *Cornus* sp., *Daphnilhyllum* sp. were reported [2)]. After Tripitaka Koreana was registered in World Cultural Heritage in 1996, identification of whole samples were demanded but non-destructive technique for identification became prerequisite. It is in such a situation that I started to investigate applicability of X-ray CT technique for wood identification.

Assuming 0.1mm resolution of a conventional CT instrument, density of the vessel distribution was mainly concerned. From the optical transverse sections of above mentioned woodblock species, the position of vessel element was obtained and their spatial distribution was analyzed by spatial point pattern analysis (Spatstat) program[3)]. Among several characteristic features obtained from this analysis, L-function was found to be the best to distinguish species tested. Although I did not have direct access to the CT images, this preliminary study suggested the potential of image analysis for non-destructive analysis of species used in Tripitaka Koreana using a conventional CT measurement.

**Acknowledgements**

I am indebted Prof. T Yoshimura, Kyoto University, for his guidance in deterioration test. I also acknowledge Prof. N-H Kim, Kangwon National University and Prof. W-H Lee, Kyungpook National University for providing samples of *P.densifrora* for. *erecta* Uyeki.

**References**

[1] H. Uyeki, On the physiognomy of *Pinus densiflora* growing in Corea and sylvicultural treatment for its improvement. Bull. Agric. & For. Coll. Suigen, Chosen, No.3, 1-263, 1928

[2] S-J. Park, A-K. Kang, Species Identification of Trioitaka Koreana. Korean J Wood Sci & Technol (in Korean) 24(3): 80-89, 1996

[3] A. Baddeley. Analysing spatial point patterns in R. Technical report, CSIRO, 2010. Version 4. Available at www.csiro.au/resources/pf16h.html.

# ABSTRACTS (MASTER THESIS)

## Analysis of interaction between carbohydrate-binding module (CBM) and lignin

**(Graduate School of Agriculture,
Laboratory of Biomass Conversion, RISH, Kyoto University)**

Mai Murakami

In lignocellulosic biorefinery, disintegration of plant cell walls by decomposing lignin network is the initial key process. Many physico-chemical, structural, and compositional factors hinder the hydrolyzability of plant cell wall polysaccharides with hydrolases. In enzymatic hydrolysis, the reaction starts from direct physical contact between the enzymes and exposed polysaccharides. However, nonspecific adsorption of enzymes on lignin decreases the reactivity, even after the rupture of the cell wall structure. Although the adsorption of cellulase to lignin depends on the structures of protein and lignin, the interactions are still poorly understood at the molecular level. Carbohydrate-binding module (CBM) of cellulase is a protein component adsorbing the enzyme on non-soluble substrates, cellulose and hemicelluloses. However, CBM also preferentially binds to lignin mainly *via* hydrophobic interaction, and the adsorbed enzyme rapidly loses its activity. Therefore understanding of the interaction between CBM and lignin is important to reduce the enzyme cost by suppression of the non-productive binding. Filamentous fungus *Trichoderma reesei* is known to be hyper producer of cellulolytic enzymes, and is widely used for commercial scale production of cellulases and hemicellulases. In this study the interactions of lignin with a fusion protein between GFP and CBMs of cellulases from *T. reesei* and bacteria were analyzed using Quartz Crystal Microbalance (QCM), and the binding properties to lignin was analyzed. Inhibition and adsorption of soluble lignin monomers, vanillic acid, syringic acid, vanillin, syringaldehyde, *p*-hydroxybenzaldehyde and *p*-hydroxybenzoic acid to cellulase are also analyzed. The results showed that the adsorption and inhibition depends on the structure of the lignin monomers. These lignin monomers inhibited adsorption of the CBM-GFP to cellulose.

# ABSTRACTS (MASTER THESIS)

## Characterization of cell wall phenylpropanoids of grass bioenergy plants

**(Graduate School of Agriculture, Laboratory of Metabolic Science of Forest Plants and Microorganisms, RISH, Kyoto University)**

Ayumi Yasui

Lignocelluloses are produced mainly by trees and large gramineous plants such as *Erianthus* spp., switchgrass, nepier grass, miscanthus etc. Generally, the biomass production by fast-growing trees such as *Cryptomeria japonica* (Japanese cedar) in Japan and *Acacia mangium* in Indonesia is about 10 and 20 tons $ha^{-1}$ $year^{-1}$, respectively, whereas that of *Erianthus arundinaceus* in Thailand and Japan reaches up to 80 and 30 tons $ha^{-1}$ $year^{-1}$. In addition, the large gramineous plants, such as *Erianthus* spp. are not used for food. Therefore, they are drawing attention as potential materials for biofuel and industrial feedstock production.

Recently, *E. arundinaceus* was characterized in detail in terms of lignins, *p*-hydroxycinnamic acids, enzymatic saccharification efficiencies, and minerals in the ash of the inner and outer parts of the internode and the leaf blade and sheath (Otake 2012; Yamamura et al. 2013). Interestingly, they found out that the inner part of the internode did not show a negative correlation between lignin contents and enzymatic saccharification efficiencies, indicating that the enzymatic saccharification efficiency of the inner part was affected by not only lignin contents but also other factors. This suggested that the lignocellulosic supramolecular structure of the inner part was different from that of the outer part. Cross-linking of grass cell wall components through diferulate residues has been known to reduce the enzymatic saccharification efficiency. However, the amounts and effect of the structure on enzymatic saccharification efficiency has not been reported for *E. arundinaceus*.

This study established a system to quantitate diferulates in cell walls of various grass bioenergy plants using a stable isotope dilution method. In this study, the author synthesized various deuterium-labeled and unlabeled diferulates (Figure 1), and showed that some diferulates are rather unstable; the unstability was partially eliminated by the introduction of protecting groups: acethylation of the phenolic hydroxyls and ethyl ester formation from the carboxyls. Diferulate **4**, which is stable, was quantified using stem of switchgrass and *E. arundinaceus* in this study, and its amount in the cell walls was found to be very small; 124 ng $mg^{-1}$ cell wall residue (CWR) in switchgrass stem, 52.2 ng $mg^{-1}$ CWR in *E. arundinaceus* inner part of internode, and negligible in *E. arundinaceus* outer part of internode. The present result suggested that the role of the diferulate residues as the obstacles of enzymatic saccharification of *E. arundinaceus* internodes may be insignificant.

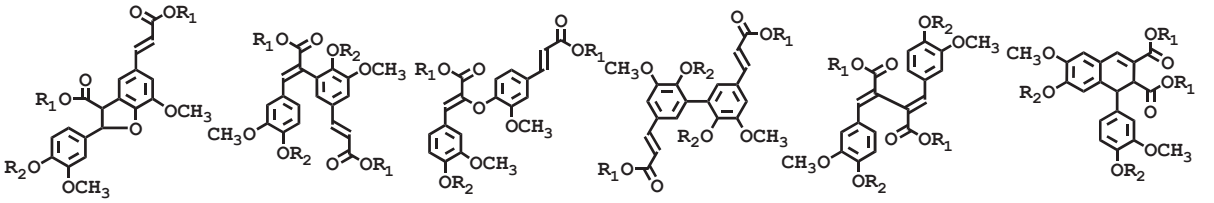


Figure 1 The structures of synthesized diferulates

### References

[1] Y. Otake, "Characterization of lignocellulose in *Erianthus ravennae*", *Master thesis*, 2012.

[2] M. Yamamura, S. Noda, T. Hattori, A. Shino, J. Kikuchi, K. Takabe, S. Tagane, M. Gau, N. Uwatoko, M. Mii, S. Suzuki, D. Shibata, T. Umezawa, "Characterization of lignocellulose of *Erianthus arundinaceus* in relation to enzymatic saccharification efficiency", *Plant biotechnology*, vol. 30, pp. 25-35, 2013.

# ABSTRACTS (MASTER THESIS)

## Biosynthetic enzymes involved in naphthalene ring formation in *Lithospermum erythrorhizon*

**(Graduate School of Agriculture,
Laboratory of Plant Gene Expression, RISH, Kyoto University)**

Yuki Takano

Higher plants produce a large number of secondary metabolites, many of which are applied for medicines, pesticides, spices, dyes, and fragrance etc. These compounds generally have complicated structures exhibiting chirality, and therefore chemical synthesis to supply these natural compounds is not cost effective in many cases. Plant cell culture system provides an effective method for stable production of valuable natural compounds. Application of plant cell cultures for production of secondary metabolite is suitable for high value compounds having a large market size, such as anticancer drugs, and/or those rarely obtained from natural sources due to the scarcity of the plants. The first example of industrial production of such a secondary metabolite by plant cell cultures was achieved in shikonin production by *Lithospermum erythrorhizon* in 1980s.

*L. erythrorhison* Sieb. et Zucc. (Boraginaceae) is a perennial herbaceous plant that is, at least in recent years, rarely found in Japan, Korea, and China. Roots of this plant appear red-purple, as its root bark (cork layers) contains a large amount of red naphthoquinone pigments, shikonin derivatives (Fig.1).

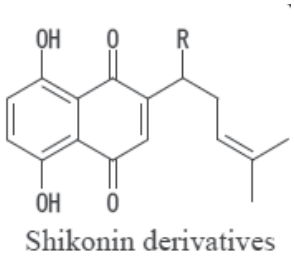


Shikonin derivatives

| Compound | R |
|---|---|
| Deoxyshikonin | -H |
| Shikonin | -OH |
| Acetylshikonin | $-OCOCH_3$ |
| Isobutylshikonin | $-OCOCH(CH_3)_2$ |
| β,β-Dimethylacrylshikonin | $-OCOCH{=}C(CH_3)_2$ |
| Isovalerylshikonin | $-OCOCH_2CH(CH_3)_2$ |
| α-Methyk-n-butylshikonin | $-OCOCH(CH_3)CH_2CH_3$ |
| β-Hydroxyisovalerylshikonin | $-OCOCH_2C(OH)(CH_3)_2$ |

Fig. 1. Shikonin derivatives detected in *L. erythrorhizon*

The cultured cells of this plant are capable of producing a high amount of shikonin derivatives in M9 medium. Its biosynthesis has been well studied on molecular level so far, while the reaction step of naphthalene ring formation from a key intermediate geranylhydroquinone is still unknown. Taking the advantage that the shikonin production is strictly inhibited by light, a subtractive hybridization experiment was done to identity enzymes responsible for the formation of naphthalene ring structure. Several genes coding for various oxidoreductases were found as being dark-inducible genes. Heterologous expression systems of the candidate clones were established with various host organisms, e.g, tobacco BY2 cells.

[1] Mizukami H, Konishima M, Tabata M, "Variation in pigment production in *Lithospermum erythrorhizon* callus cultures," *Phytochemistry*, vol. 17, pp. 95-97, 1978.

[2] Fujita Y, Hara Y, Suga C, Morimoto T, "Production of shikonin derivatives by cell suspension cultures of *Lithospermum erythrorhizon*. 2. A new medium for the production of shikonin deivatives," *Plant Cell Rep*, vol. 1, pp. 61-63, 1981.

[3] Yamamoto H, Zhao P, Yazaki K, Inoue K, "Regulation of lithospermic acid B and shikonin production in *Lithospermum erythrorhizon* cell suspension cultures." *Chem. Pharm. Bull.*, vol. 50, pp. 1086-1090, 2002.

# ABSTRACTS (MASTER THESIS)

## An observational study on the time and spatial variations of precipitable water vapor with a dense GNSS receiver network

**(Graduate School of Informatics,
Laboratory of Atmospheric Sensing and Diagnosis, RISH, Kyoto University)**

Yuya Iwaki

The integrated amount of water vapor along the zenith angle, or PWV (Precipitable Water Vapor) can be estimated by GPS (GNSS) meteorology, which is a method to compute atmospheric parameters from troposphere-induced delays in signals of GPS (GNSS). We deployed a dual-frequency (DF) GNSS network around Uji campus of Kyoto University, Japan, with inter-station distances of few kilometers. By using this network, we built a basic system to observe PWV fluctuations occurring within a small horizontal scale (less than 10 km), which were then analyzed to identify possible precursors of local torrential rain.

We analyzed the variation of PWV on July 9 and 25, 2012, when localized heavy rain was observed. Both the averaged value and the variance of PWV between GNSS stations increased before a nearby meteorological radar detected the rain clouds. In the latter case, the difference of PWV among stations increased at most 5 mm.

For utilizing this network as a practical heavy rain early warning system, real-time satellite orbit and clock products are required. By introducing correcting method of predicted satellite clock information, the difference between the real-time PWV and that obtained in post processing by means of precise orbit and clock products for post processing was 1.5 mm in RMSE.

To build a dense GNSS network over urban areas, the usage of inexpensive single-frequency (SF) receivers would be beneficial for economic reasons. We implemented software to correct the effect of ionosphere delays on SF observations, according to a method called SEID. By applying SEID for SF PWV retrieval, the error in terms of PWV with respect to the DF solution was about 1.6 mm in RMSE. The PWV horizontal distribution obtained by SF analysis with this model could detect localized PWV inhomogeneity emerging prior to a rainfall which occurred within a small horizontal scale less than 3 km.

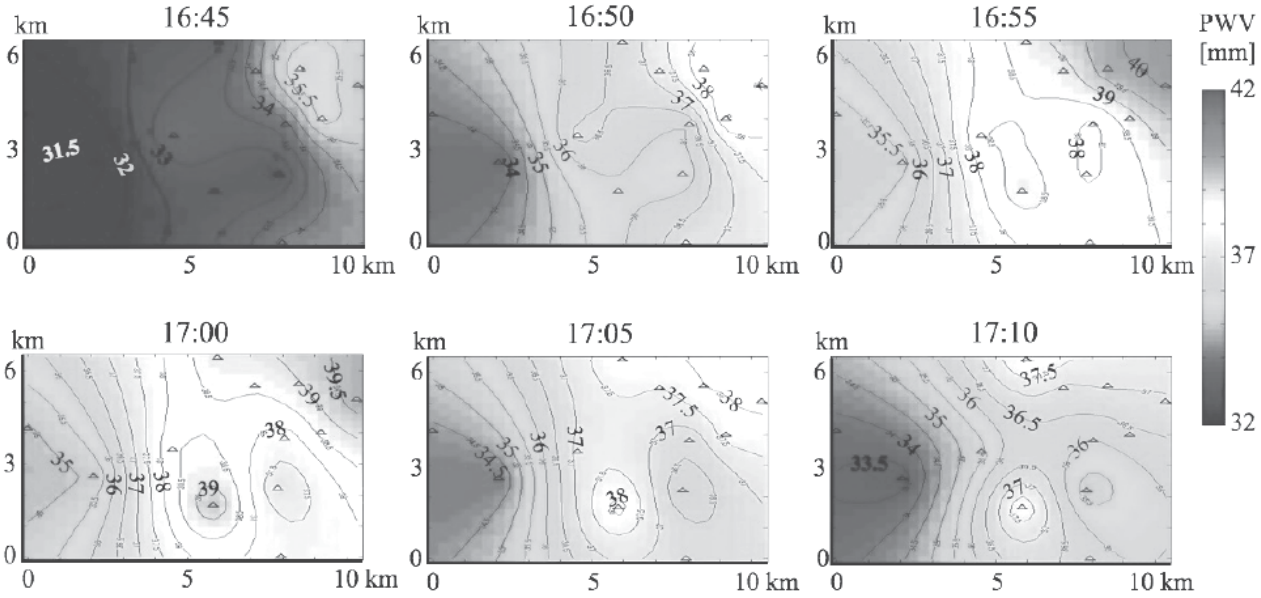


Figure 1. Horizontal distribution of precipitable water vapor (PWV) observed by a dense GNSS receiver network around Uji campus of Kyoto University on July 9, 2012.

# ABSTRACTS (MASTER THESIS)

## Study of Medium Scale Traveling Ionospheric Disturbance with Sounding Rockets and Ground Observation

**(Graduate School of Informatics, Laboratory of Radar Atmospheric Science, RISH, Kyoto University)**

Tomohiro Kato

In the midlatitude ionospheric F-region, mainly in summer, wave structures of electron density that have wave length of 100-200 km and period of one hour are observed. This phenomena is called Medium Scale Traveling Ionosphiric Disturbance; MSTID. MSTID has been observed by GPS receiver network, and its characteristic were studied. In the past, MSTID was thought to be generated by the Perkins instability, but its growth ratio was too small to be effective. Recently coupling process between ionospheric E- and F- regions are studied by using two radars and by computer simulations. Through these studies, we now have hypothesis that MSTID is generated by the combination of E-F region coupling and Perkins instability. To clarify this hypothesis, an experiment using two sounding rockets (S-520-27 and S-310-42) was conducted. The rockets are launched on July 20, 2013 from JAXA Uchinoura Space Center. Rockets have several equipments, and observe electric field, electron density, etc. In this thesis, the electric field of E- and F region is analyzed. The method and principle of estimating natural electric field is explained. By applying this method to a previous rocket (S-520-26) that was launched in January 2012, the method is confirmed to be correct, and the value of the natural electric field was nearly 1mV/m. In the experiment of S-520-27, the natural electric field ranged about − 5mV/m, and the time variation from southeast ward to east ward, and period of 100 seconds (Figure 1). The Pedersen conductivity is estimated by the observation of electron density. By using this, the electric field was mapped to the horizontal plane at 280km height along the geomagnetic field line. By comparing with GPS-TEC, the correlation between the natural electric field and TEC variation was found. From the above, in this thesis, the vector of electric field in MSTID is estimated and the characteristic of polarization electric field is elucidated.

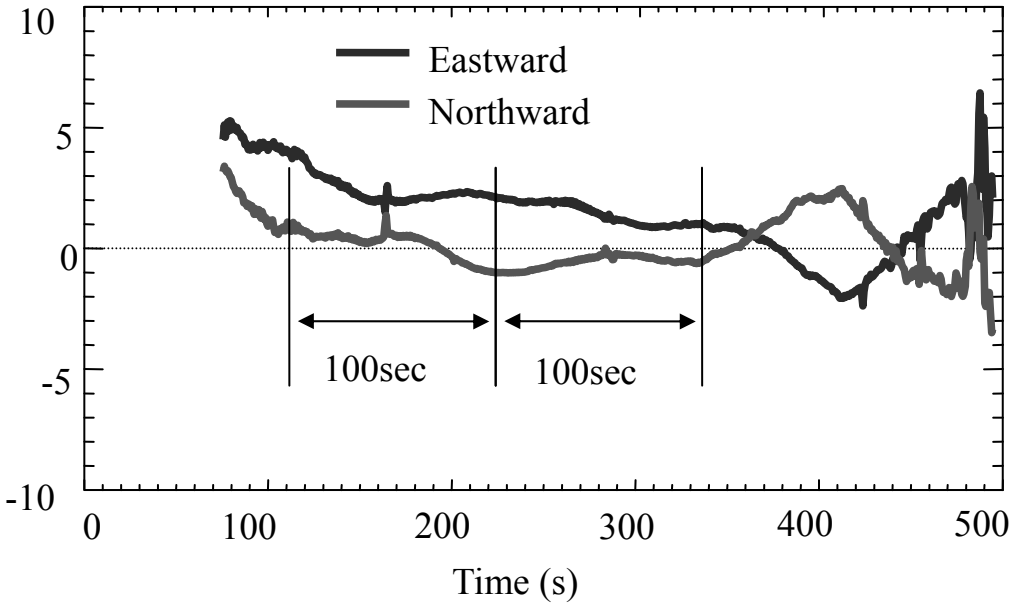


Figure 1: Electric field time variation measured by the double-probe on board of S-520-27 sounding rocket.

# ABSTRACTS (MASTER THESIS)

## Development of a thermoplastic nanocomposite using a wood cell wall nanostructure

**(Graduate School of Agriculture,
Laboratory of Active Bio-based Materials, RISH, Kyoto University)**

Yuta Watanabe

### Introduction

Wood cell walls are natural nanocomposites. Cellulose nanofibers (CNFs) are fillers and hemicellulose and lignin are matrix substances. The wood cell wall structure is well-ordered at the nanoscale and CNFs have significant advantages as fillers including high strength and low thermal expansion properties that derive from the extended cellulose molecular chain crystal structure. Hence, the development of a novel thermoplastic material using the wood cell wall nanostructure was studied.

For this purpose, CNF covered with lignin (lignoCNF) was prepared and a selective chemical modification of the hydroxyl group of lignoCNF was carried out. The aim was to enhance the thermoplasticity of the matrix without damaging the cellulose crystal structure.

### Materials and Methods

LignoCNF was prepared from softwood Bleached Chemi-ThermoMechanical Pulp (BCTMP) using a grinder, based on a previous report[1)]. After solvent displacement into N-methylpyrrolidone, in the presence of pyridine, esterification using acetic anhydride and n-octanoyl chloride was performed at 60°C for 12h. Different degrees of substitution (DS) of the esterified lignoCNF were obtained by changing the amount of reagent. The samples were freeze-dried and compression molded at 160°C or 200°C. The crystallinity, dynamic viscoelasticity and linear thermal expansion of the molded samples were studied using X-ray diffractometry (XRD), Dynamic Mechanical Analyses (DMA) and Thermo-Mechanical Analyses (TMA), respectively.

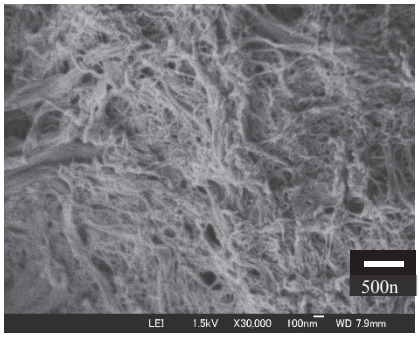

Figure 1. FE-SEM image of lignoCNF.

### Results and Discussion

LignoCNF of 20 nm to 1 μm in size was obtained after 3 passes of grinder treatment (Figure 1). This lignoCNF contained 25% lignin (klason lignin), which is similar to the original softwood.

Esterification improved the thermoplasticity of the lignoCNF. Upon octanoylation treatment, the thermoplasticity was drastically improved above DS=0.6, which means that 20% of the surface hydroxyl groups of the lignoCNF were substituted (Figure 2a and c). However, its thermal expansion was quite high. In the case of acetylation, the substitution of 30% of the hydroxyl group (DS=0.8) enabled a close adhesion between the lignoCNF elements after compression at 200°C and 50MPa (Figure 2b and d). The crystal structure of the CNFs was maintained and a low coefficient of thermal expansion (CTE) of 30 ppm/K was obtained, which is similar to the CTE of aluminum alloys.

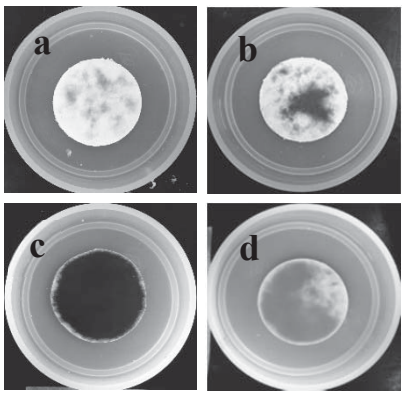

Figure 2. After compression molding at 50MPa. a : untreated, 160°C, b: untreated, 200°C, c : octanoylation(DS=0.6), 160°C, d : acetylation(DS=0.8), 200°C.

### References

[1] Abe, K, F. Nakatsubo and H. Yano, "High-strength nanocomposite based on fibrillated chemi-thermomechanical pulp," *Composite Science and Technology*, vol. 69, no. 14, pp. 2434-2437, 2009.

# ABSTRACTS (MASTER THESIS)

## Measuring stress by biogenic amine analysis using LC/MS with a subterranean termite *Coptotermes formosanus* Shiraki

**(Graduate School of Agriculture, Laboratory of Innovative Humano-habitability, RISH, Kyoto University)**

Kazuhiro Hirata

### Introduction

Stress response has been widely studied and become one of the more important research topics in entomology. There have been few reports, however, on the stress response of wood-attacking insects such as termites. The influence of the homeostasis disturbance caused by stress affects the behavior and mortality of insects. Thus, the impact of stress should not be disregarded in bioassays of termites.

The purpose of this study was to establish the protocol for measuring stress in termites. Biogenic amines, dopamine and octopamine were target chemicals, measured by liquid chromatography-mass spectrometry (LC/MS). The two amines had the same molecular weight of 153.18, and the special protocol was indispensable for LC/MS analysis.

### Materials and methods

Mature workers of a subterranean termite (*Coptotermes formosanus* Shiraki) were collected from a laboratory colony maintained in the Deterioration Organisms Laboratory (DOL), RISH, at Kyoto University. The insects were exposed to 4 kinds of stresses: physical (vibration), nutritional (starvation), social (isolation) and physical/social (isolation by a stainless-mesh). They were then killed quickly by dipping into liquid nitrogen, and their brains were carefully collected with a pair of fine forceps. The brains were deproteinized by the mixing ethanol precipitation-centrifugation method, and the obtained samples served for LC/MS analysis.

### Results and discussion

By investigating many combinations of mobile phases and columns, a protocol for analyzing dopamine and octopamine in the termite brain was established. Octopamine and dopamine were successfully separated from the samples by this protocol, and were quantitatively analyzed. The brains of the freshly collected *C. formosanus* workers contained high levels of octopamine and low levels of dopamine.

When the termites experienced stress, octopamine levels were significantly decreased, regardless of stressor. In contrast, dopamine level change depended on the stressor. Dopamine level was increased by vibration (physical stress), decreased by starvation (nutritional stress), and did not change by isolation (social stress). Interestingly, when facing combined stress (physical/social stresses by isolation), the insects showed a combined reaction against the two stresses. Octopamine levels were more stable than those of dopamine. The results were consistent with those of other insects such as German cockroaches.

Breeding with more than 5 individuals can reduce stress in termites. This clearly shows stress relaxation by chemical communication with nest mates in termite societies, suggesting that results of laboratory bioassays, such as evaluation of the termiticidal effectiveness of chemicals and anti-termite performance of building materials, might depend on the population of test insects. Collecting data on the relationships between other biogenic amines and other types of stressors will help us understand the physiology of termites, an extremely economically important insect, in more detail.

### Acknowledgement

The author deeply thanks Dr. Hiroshi Nishimura, Laboratory of Biomass Conversion, RISH, Kyoto University for his support with the LC/MS analysis. Appreciation also goes to Termi-mesh Japan Co. Ltd, and Kansai Wire Netting Co. Ltd for providing the high-quality stainless mesh samples as physical barriers.

# ABSTRACTS (MASTER THESIS)

## X-ray Computer Tomographic Analysis of Breeding Chambers and Gallery Systems in Wood Created by a Drywood Termite, *Incisitermes minor* (Hagen)

**(Graduate School of Agriculture,
Laboratory of Innovative Humano-habitability, RISH, Kyoto University)**

Khoirul Himmi Setiawan

**Introduction**

The western drywood termite, *Incisitermes minor* (Hagen) (Kalotermitidae), is considered to be the most destructive drywood termite in the western United States (USA). Today, more than half of the prefectures in Japan are also listed as infested areas. Despite it being an economically important pest, the nesting biology of *I. minor* is poorly understood. To date, there are no published data available regarding *in situ* nest-gallery development of *I. minor*. In the present study, two commercial timbers, Sitka spruce (*Picea sitchensis* Bong. Carriere) and Sugi (*Cryptomeria japonica* D. Don), were used to evaluate nest-site selection and nest-founding activity in *I. minor*.

**Materials and Methods**

Forty Sugi and 60 Spruce timbers were prepared; sample dimensions were 50 mm (R) x 50 mm (T) x 1000 mm (L), and each included sapwood and heartwood portions. All timbers were placed in highly infested attic areas at four different houses in the Wakayama Pref., Japan. CT-scan analysis of samples was carried out with a large-scale X-ray CT apparatus (YXLON International GmBH Germany) at the Kyushu National Museum, and the data were reconstructed into three dimensional (3-D) images, 2-D section images, and series of virtual cuts using volume graphics software (VGStudio MAX 2.1, Volume Graphics GmbH Germany: digital data thickness 1 mm, 1024 x 1024 pixels, 3.17 2-D image slice per mm).

**Result and Discussion**

The results indicated that *I. minor* showed a preference for the spruce timbers over the Sugi timbers in establishing the first royal cells. To observe the breeding chambers and nest-gallery development, three spruce timbers were selected for bi-annual analyses by X-ray CT. Two timbers were infested by five pairs of reproductives from nuptial flight. Other timber was infested by the outside foraging of a group of individuals that emerged from the natal nest. CT images revealed that *I. minor* reproductives showed anatomical selectivity in both nest-founding activity and nest-development. The structure of the initial chambers varied to follow to the anatomical texture of the wood; resembled either a pear-shape or cashew nut-shape. The first six-month CT analyses indicated two kinds of strategies to initiate a new colony. In the first, two of the reproductive pairs expended energy in brooding, while simultaneously curtailing foraging; the other three pairs concentrated on foraging. The reproductive pairs showed no hibernation period and continuously excavated the galleries during the first six months. The nest-gallery was excavated cavernously in a particular annual growth ring where the breeding chamber was established. All the chambers showed significant accretion in volume and structure. After one year, one reproductive pair had exhibited no brooding activity, while the other four had 2 - 5 new colony members.

The infestation by a group of individuals demonstrated the different pattern of nest-development to that of the nuptial flight. The group established the first chamber, which was transversely excavated across several growth rings. After one year, the nest-gallery systems had been established consisting of seven chambers with extensive galleries across both sapwood and heartwood. Young colony members were observed, which indicated the emergence of the replacement reproductives. Although drywood termites have been classified as having the most primitive nesting behavior, the current results indicated that nest excavation of a one-piece nester involves quite intricate environmental responses.

**Acknowledgments** The author thanks to Mr. Akio Adachi, Dr. Yoshiyuki Yanase, Dr. Takuro Mori (Kyoto Univ.); Mr. Masao Oya (Oya Shiroari Giken); Mr. Toshiyuki Torigoe (Nara National Museum), Dr. Setsuo Imazu (Kyushu National Museum) for their contribution on the study.

# ABSTRACTS (MASTER THESIS)

## Molecular Phylogenetic Analyses of Fungal Diversity in Agarwood from *Aquilaria malacensis*

**(Graduate School of Agriculture, Laboratory of Innovative Humano-habitability, RISH, Kyoto University)**

Munadian

**Introduction**

Agarwood (known as Jinko in Japan), a dark resinous wood found in trees in Southeast Asia such as *Aquilaria* sp., has been traditionally used for incense and perfumes, and thus it has been considered a high-value non-timber forest product. Since agarwood is a biological product of the defensive reaction against fungal infection, a human-inducible stimulus that mimics the natural fungal infection phenomenon in trees is necessary for the industrial production of agarwood. The artificial formation of agarwood by forcible infection using a specific fungus may be a useful option for the industrial production of this wood. For this purpose, identification of the fungus responsible for agarwood formation is needed, but the information available on isolating this fungus is limited. In the present study, the fungal community existing in agarwood of *Aquilaria* sp. was investigated by polymerase chain reaction - denaturing gradient gel electrophoresis (PCR-DGGE) and was compared with that in healthy wood of *Aquilaria* sp. to identify the fungus that causes agarwood formation.

**Materials and methods**

Eight wounded *Aquilaria malacensis* trees (T1-T8) were selected from two different islands in Indonesia (Sumatra and Kalimantan Island). Genomic DNAs were extracted from 90 mg of milled wood samples using the DNeasy Plant Mini Kit (Qiagen). PCR was done in a reaction volume of 50 µl containing 2 mM of dNTPs, 25 mM $MgSO_4$, 10 x PCR buffer for KOD ver. 2, 1 U of KOD plus ver. 2 DNA polymerase, 10 µM of primers (ITS1-F and ITS4), and the extracted genomic DNA already mentioned. After the reaction, PCR products were analyzed by electrophoresis on 1% agarose gel and then underwent DGGE analysis using 8% polyacrylamide gel containing a 20-70% concentration gradient of denaturant. The separated DNA fragments were subjected to sequencing analysis. The determined nucleotide sequences were used for a BLAST search using the blastn algorithm at the NCBI website.

**Results and discussion**

When the PCR products were subjected to DGGE analysis, a total of 124 DNA bands were separated based on their different levels of mobility on the gel for the samples from Kalimantan. Among these DNA bands, the nucleotide sequences of 56 DNA fragments (37 fragments from dark wood and 19 fragments from white wood) were identical with those from filamentous fungi. Under conditions similar to those for the Kalimantan samples, the Sumatra samples were subjected to DGGE analysis; 85 of the DNA bands were separated, and among them 40 of the DNA fragments including 29 fragments from dark wood and 11 DNA fragments from white wood were also identical with those from filamentous fungi. In this study, Ascomycetes and Basidiomycetes were discovered in both areas. This study shows the advantages of the DGGE technique. PCR-DGGE obtained overall data on the fungi species that exist in natural agarwood. Other studies reported that several fungi were isolated from agarwood. In the present study, we identified more fungal species, suggesting that agarwood might be formed by the association of multiple fungi.

**Acknowledgements**

I would like to express my deepest gratitude to Dr. Makoto Yoshida and Dr. Yuji Nakada of Tokyo University of Agriculture and Technology for their help with this study.

# ABSTRACTS (MASTER THESIS)

## Research on rapid increases of oxygen ion flux in the inner magnetosphere during the substorms

**(Graduate School of Electrical Engineering, Laboratory of Space Radio Science Simulation, RISH, Kyoto University)**

Yohei Nakayama

Many charged particles are trapped in the magnetosphere where the Earth's dipolar magnetic field dominates the external magnetic field. Plasma population and flux are dramatically changed during magnetic storms and substorms. Rapid enhancements of energetic ions during a substorm are one of the unsolved issues in the inner magnetospheric research (< 7 Re). Previously, two distinct processes have been suggested to explain the enhancements. The first one is transport from the near-earth plasma sheet, and the other one is local acceleration. To test the both process, we performed test particle simulation under the electric and magnetic fields that are self-consistently obtained by the global MHD simulation developed by Tanaka et al. [1].

We released oxygen ions in tail region with an interval of 1 minute. The distribution function in the lobe is assumed to be drifting Maxwellian. The temperature is assumed to be 10 eV, the density is $10^5$ $m^{-3}$, and the parallel velocity is given by the MHD simulation. In total, a few hundreds of millions of particles are traced. Each test particle carries the real number of particles in accordance with the Liouville theorem. After tracing particles, we reconstructed 6-dimensional phase space density of the oxygen ions, as well as the directional differential number flux using the phase space mapping so as to be able to make a direct comparison with in-situ satellite observations.

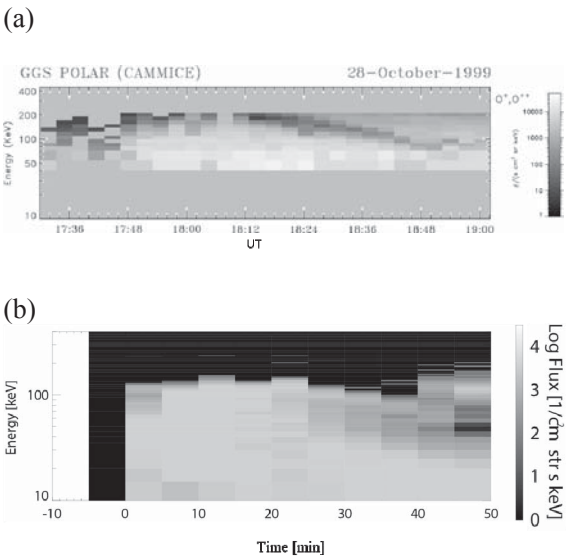


Figure 1. Energy versus time spectrograms of differential flux of energetic oxygen ions (a) observed by the Polar satellite, and (b) reconstructed by our simulation.

Just after a substorm onset, the differential flux of the ions is rapidly enhanced in the energy range from 50 to 150 keV at radial distance R greater than 7 on the nightside in the equatorial plane. The region of the enhanced flux propagates duskward, then to dayside because of grad-B and curvature drift of the ions. We also plotted energy versus time spectrograms of the differential flux at a fixed position, and compared with the Polar satellite observation (Figure 1). At 7.2 Re and at 22.4 MLT, the ion flux is suddenly enhanced about 10 minutes after the onset. The enhancement appears first at 120 keV, followed by lower energy as time proceeds. After a while, a high energy ion flux appears first, followed by that at lower energies. This is a called a drift echo, arising from the ions that encircled the Earth by the grad-B and curvature drift.

We successfully simulated the similar energy-time dispersion observed by Polar, and investigated the transport and acceleration processes and the dependence of the flux on the source distribution function.

### References

[1] Tanaka, T., A. Nakamizo, A. Yoshikawa, S Fujita, H. Shinagawa, H. Shimizu, T. Kikuchi, and K. K. Hashimoto, "Substorm convection and current system deduced from the global simulation", *J. Geophys. Res*. 115, A05220, doi:10.1029/JA014676, 2010.

# ABSTRACTS (MASTER THESIS)

## Study and Development of an Intermittent Microwave Power Transmission System for ZigBee Devices

**(Graduate School of Engineering,
Laboratory of Applied Radio Engineering for Humanosphere, RISH, Kyoto University)**

Takuya Ichihara

The objective of the present thesis is to develop a microwave power transmission (MPT) system for ZigBee device, shown in Figure 1, in order to realize wireless and battery-less sensor network. For saving on the frequency resources, it is recommended that the frequency of MPT system be in the same frequency band as that of ZigBee communication. In the case, however, the MPT would interfere with the ZigBee communication, and ZigBee devices would get disabled to communication. To solve the interference problem between MPT and ZigBee communication, we propose intermittent MPT, which is the method that microwave is irradiated for power supply while the ZigBee devices sleep. In the previous studies, we confirmed that a ZigBee device worked and communicated correctly by intermittent MPT without a battery. However, it is concerned that communication interference with MPT would occur stochastically without any scheduling rules. Therefore we develop a way of scheduling management between ZigBee communication and MPT in the present thesis. First, we developed the transmission scheduling program. The scheduling program successfully worked on the system with a single ZigBee device with battery drive. Next, we improved the power receiving devices. We developed a rectifying circuit with a slave circuit. The RF-DC conversion efficiency of the rectifying circuit was 58 % with the wide range of the output load from 150 ohm to 1100 ohm. Thus, we improved the total RF-DC conversion efficiency of rectifying circuit from 27.5 % to 55.7 %. We also developed an estimation program for selecting the size of capacitors. Then, with the developed scheduling program and improved receiving device, we conducted the intermittent MPT demonstration for both a single and two receiving circuits and ZigBee devices, as shown in Figure 2. Finally, we successfully conducted the demonstration for 24 minutes in the case of a single ZigBee device and for 74 minutes in the case of two ZigBee devices.

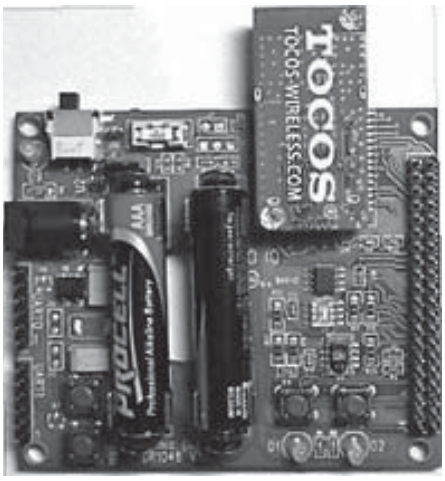


Figure 1. ZigBee device.

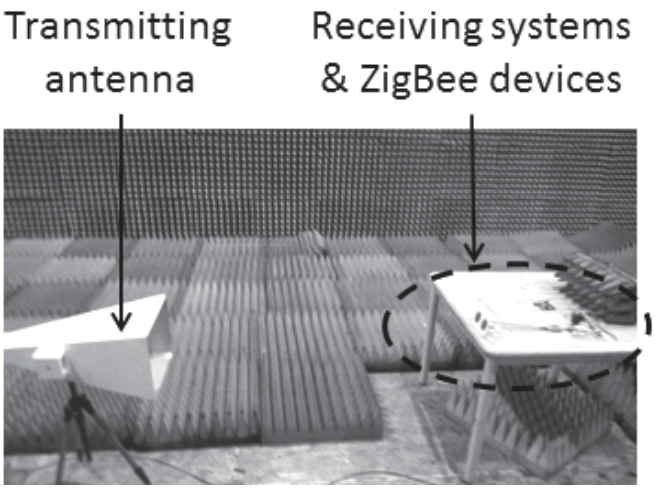


Figure 2. Demonstration of intermittent MPT for two receiving systems and ZigBee devices.

# ABSTRACTS (MASTER THESIS)

## Fundamental Study of a Small-Size and Large-Effective-Aperture Antenna by using Spherical Dielectric Resonator

**(Graduate School of Engineering,
Laboratory of Applied Radio Engineering for Humanosphere, RISH, Kyoto University)**

Takayuki Matsumuro

Recently, another type of the Solar Power Satellite (SPS) system, "ubiquitous SPS system" has been proposed. In this system, microwave energy from the space is distributively received and directly supplied for social infrastructures, such as street lights and base stations of mobiles. In the ubiquitous SPS system, power density is restricted to 10 W/m$^2$ for human safety. Limited power density requires antennas with large directional gain to receive enough power for devices. It causes problem of the miniaturization of antennas, because the directional gain is proportional to the physical size in the case of aperture antennas. To solve this problem, this research focuses on spherical wave expansion of a plane wave as a new method of realizing compact high-gain antennas. Spherical wave expansion is used for the analysis method of small antennas, directional antennas and antenna measurement, but it is not used for the design method of antennas yet. Therefore, in this paper, the design method of compact high-gain antenna based on the principle of spherical wave synthesis is investigated for the efficient microwave power transmission. First, in the present research, we have analyzed the directivity of the synthesized spherical wave, which is obtained by synthesizing a set of spherical waves with the expansion coefficient of a plane wave. The electromagnetic field of each order of spherical wave is given by corresponding order of the spherical Bessel function and the spherical harmonics. Figure 1 indicates calculation results on the directivity of the synthesized spherical wave. Next, we have investigated the structure of a radiation element of synthesized spherical wave. Since wave sources of the synthesized spherical wave are multi-poles, which are put at the same one point, radiation elements with finite size are required in order to realize a practical antenna. For this problem, we have revealed that a spherical dielectric resonator can work as the accurate wave source of a spherical wave with any order mode. Then, we have proposed the multilayered spherical dielectric resonators as a radiation element of the synthesized spherical wave. Synthesized spherical waves are composed of the orthogonal set of the several modes of spherical wave. In order to synthesize these modes, the resonant frequencies of the corresponding modes of the radiation element should be degenerated. For this problem, a prospect of degeneracy is given by the multilayered spherical dielectric resonators. Finally, we have made a homogeneous spherical dielectric resonator and have experimentally measured its resonance characteristics with rectangular waveguide.

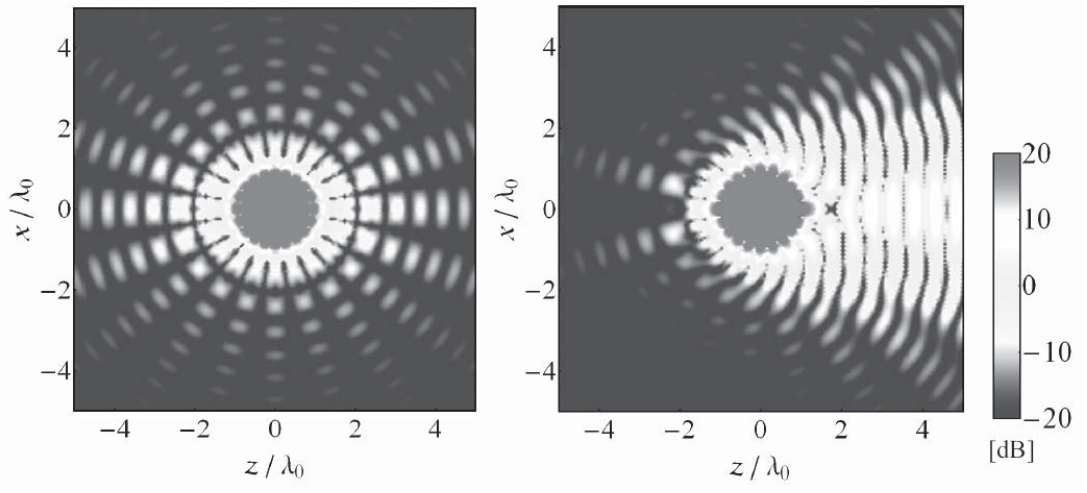


Figure 1. Calculation results on the directivity of the synthesized spherical wave.

# ABSTRACTS (MASTER THESIS)

## Research on Rectenna Rectifier for Wireless Power Transmission Application to High Speed Wireless Communication System

**(Graduate School of Engineering,
Laboratory of Applied Radio Engineering for Humanosphere, RISH, Kyoto University)**

Ryosuke Narasaki

The objective of the present thesis is to design rectenna rectifier for wireless power transmission application to high speed wireless communication system. Nowadays, they propose a high speed wireless communication system at 60 GHz utilizing repeaters across the wall. A repeater is inside of a building and the other is outside. Wireless power transmission technology can be utilized for supplying electricity from the inside repeater to the outside. We design a 60 GHz rectifier to realize high speed communication and wireless power transmission in the same frequency band. First we applied a design method of the 24 GHz-band rectifier, which was developed in the previous study, to 60 GHz-band rectifier. We adopted a microstrip line as a transmission line. We selected the Teflon substrate of 0.1mm thickness and set the width of the center conductor narrow in order to suppress the effect of the surface wave to conduct accurate simulation in ADS (Advanced Design System). Then we modeled end launch connector and microstrip line to conduct simulation in ADS more precisely. Then the rectifier achieved the efficiency of 20.7 % in the simulation. Second, we improved RF-DC conversion efficiency of the rectifier. We improved a length of the transmission line between the anode terminal and the through hole to decrease propagation loss. The improved rectifier we designed achieved the efficiency of 46.2 % in the simulation when input power was 80 mW. We clarified the reason why improvement of the line length increased the efficiency by an equivalent circuit. Finally we designed single-series rectifier. The rectifier achieved the efficiency of 45.3 % when input power was 40 mW. The simulation result of power loss ratio on a designed rectifier is shown in Figure 1. We succeeded in reducing the input microwave power without degradation of RF-DC conversion efficiency.

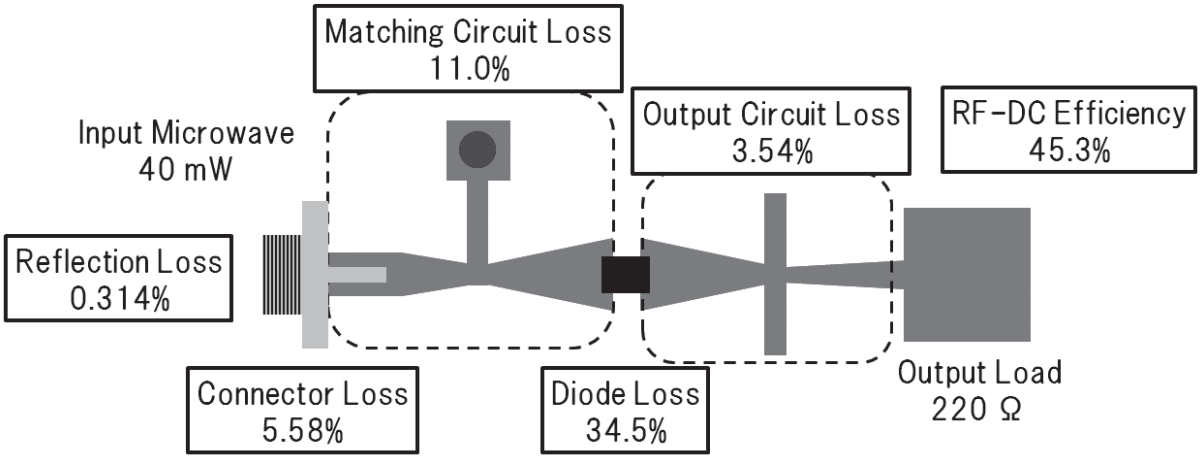


Figure 1. Simulation result of power loss ratio on a rectifier.

# ABSTRACTS (MASTER THESIS)

## Study on Antennas Appropriate for Low-Power Rectennas in Microwave Power Transmission

**(Graduate School of Engineering, Laboratory of Applied Radio Engineering for Humanosphere, RISH, Kyoto University)**

Yan Zhou

In recent years, microwave power transmission has drawn our attention, which can be used in low power driving devices aiming at battery free. However, the starting voltage of a diode leads to the RF-DC conversion inefficiency of a low input rectenna. Through prior research, some methods were used to improve the RF-DC conversion efficiency by enhancing the applied voltage to a diode. We proposed two methods; one was to improve the impedance of the rectenna and the other was to design the high Q value antenna. In the first place, we investigated the characteristics of various antennas. Then we chose patch antennas to do the following research because they were easy to be manufactured and had a high directional gain. After that, we discussed the efficiency of low-power rectennas with high impedance. To begin with, we used ADS simulator to do the simulations of the rectifying circuits with characteristic impedance between 50 ohm and 400 ohm. We proved that the efficiency of the rectifying circuit can be improved by raising characteristic impedance. Then, we fabricated the rectifying circuits whose characteristic impedance was 50 ohm, 70 ohm, 80 ohm, 90 ohm and 100 ohm, respectively, as shown in Figure 1. From measurement results, we obtained the highest efficiency at the impedance of 80 ohm, the efficiency of which was 13% higher than the conventional 50 ohm rectifying circuit. Then we designed the high impedance patch antennas. When the impedance improved, the characteristics of antennas were almost the same. Consequently, we will connect the high impedance antenna with a diode directly to improve the voltage of the diode moreover in the future. Next, we measured efficiency of low-power rectenna with high Q value. We used two measuring systems. In one measuring system, we obtained higher conversion efficiency with a low Q value antenna, but which had a small reflection loss. In the other measuring system, we obtained the same conversion efficiency of all species. Then we analyzed the reason to find out only the series resonance circuit can obtained a high voltage when the resistance was settled in the circuit. To design a series resonance circuit with high Q value will be a future problem.

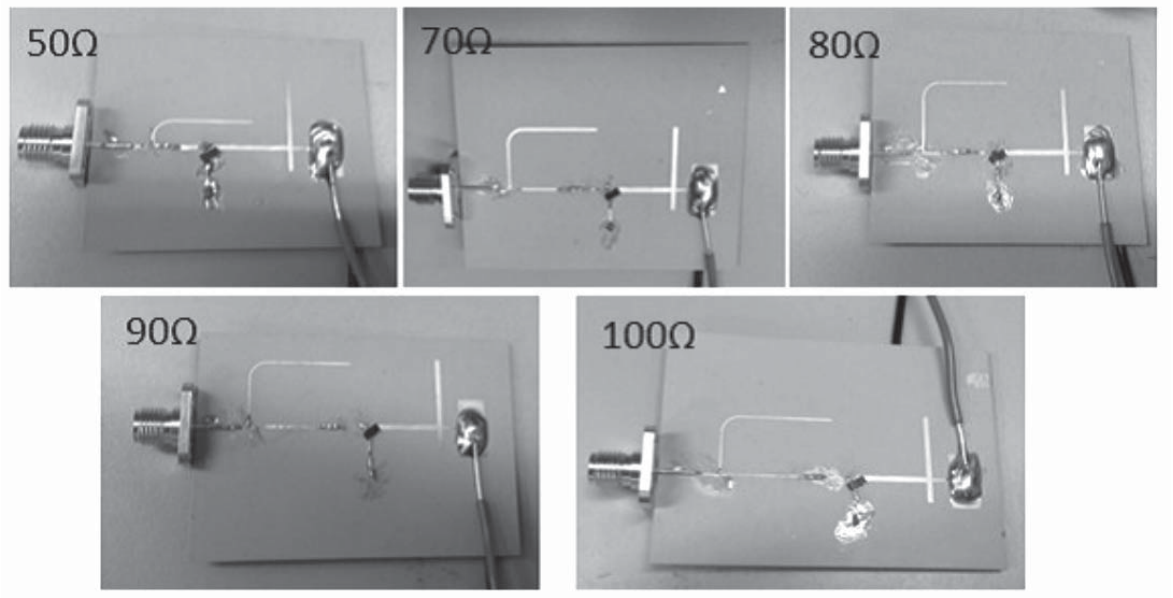


Figure 1. Rectifying circuits with various characteristic impedances.

# ABSTRACTS (MASTER THESIS)

## Study on Minituarization of Sweep Frequency Analyzer for Observation of Space Electromagnetic Environment

**(Graduate School of Engineering, Laboratory of Space Systems and Astronautics, RISH, Kyoto University)**

Kensuke Hangyo

This thesis presented our attempt toward realizing a small-size Sweep Frequency Analyzer (SFA) using the ASIC (Application Specific Integrate Circuits). To get information on energy exchange process between plasma waves and particles, very small SFA is essential. In our previous study, components for SFA such as Phase Locked Loop (PLL) and Band Pass Filter (BPF) were designed and manufactured. However, each component did not operate as we designed and satisfy the required specifications. In this thesis, we studied the reason why the BPF and PLL which have manufactured in present study didn't operate as designed and redesigned these components. After discussing the problem of the previous study, we discussed the performance of each component and frequency conversion circuit. First, we studied the reason why the manufactured BPF was unstable and didn't have enough attenuation. It was because that the switching frequency of the BPF was 10 MHz which was higher against working speed of the used op-amp. By changing this switching frequency from 10 MHz to 2:5 MHz, we realized a stable BPF. In addition, by improving the measurement environment, the BPF can realize high attenuation. Moreover, we found that the lower attenuation of the manufactured BPF was due to the switching noise of the BPF. Regarding the PLL, we addressed the problem that it could not oscillate lower frequency signals. We found that the Voltage Controlled Oscillator (VCO), which worked in the PLL, also could not oscillate lower frequency signals. This was because that the OTA which was used in the VCO did not work as we designed. Moreover, we also found that the spectrum of the oscillation signal of PLL was too broad to work in the SFA. Finally, we manufactured these circuits in a one-chip and conducted performance test. We succeeded frequency conversion of the observation wave. In addition, when it comes to the frequency conversion part which composed of the mixer and the BPF, we succeeded to reach the dynamic range of 60dB.

# ABSTRACTS (MASTER THESIS)

## Orbital Deflection of Potentially Hazardous Asteroids Using Space Environment

**(Graduate School of Engineering,
Laboratory of Space Systems and Astronautics, RISH, Kyoto University)**

Kouhei Yamaguchi

The aim of this study is to propose methods to deal with the potential threat posed by the asteroid with Earth collision probability.

The first method is a kinetic energy impactor (KEI), which impacts an asteroid with a projectile at a high relative velocity to deflect the asteroid. Our capabilities of deflecting such asteroid would be constrained by a reaction mass of a propulsion system. To solve this problem, we assumed an electric solar wind sail (E-sail) as a propulsion system. The E-sail uses the solar wind dynamic pressure to produce a continuous thrust without consuming fuel. To calculate the orbital motion of the E-sail, we proposed a calculation model considering the relations between E-sail attitude and its thrust direction. In addition, we suggested a new orbital maneuver not changing sail plane's angle but controlling thrust magnitude. Trajectory optimizations for E-sail KEI were performed on a fictional impact scenario, which was comprised of a million tons of asteroid detection on January 1, 2015, and the Earth impacting on January 1, 2030. The results showed that the projectile could yield the relative impact velocity up to 14 km/s and cause the deflection distance of 8000 km at the predicted Earth collision date.

As a second method, we studied a Coulomb force attractor, which tows the asteroid by means of Coulomb force produced by artificially charging both a spacecraft and the asteroid. By introducing the results of previous study, such as charging technique for the asteroid and magnitude of Coulomb force, we formulated the dynamics of the problem. Through numerical simulations, the performance of the Coulomb force attractor was examined. The results showed that a 500 kg spacecraft charged to 20 kV could achieve about 800 m change in orbit of a million tons of asteroid charged to -20 kV with a completion time of 1 year. This value was about 1.3 times better than the result of traditional gravity tractor. By performing this simulation for the fictional impact scenario, the resulting deflection distance was also investigated. The deflection distance became about 6 km and this value would be enough for performing the pre gravitational keyhole deflection missions, which make the asteroid orbit away from the small region.